Journal of Rock Mechanics and Geotechnical Engineering 14 (2022) 1588–1608

Contents lists available at ScienceDirect

Journal of Rock Mechanics and Geotechnical Engineering

journal homepage: www.jrmge.cn

Full Length Article

Novel integration of extreme learning machine and improved Harris hawks optimization with particle swarm optimization-based mutation for predicting soil consolidation parameter

Abidhan Bardhan [a,*], Navid Kardani [b], Abdel Kareem Alzo'ubi [c], Bishwajit Roy [d], Pijush Samui [a], Amir H. Gandomi [e]

[a] Department of Civil Engineering, National Institute of Technology Patna, Patna, 800005, India
[b] Discipline of Civil and Infrastructure Engineering, School of Engineering, Royal Melbourne Institute of Technology (RMIT), Melbourne, VIC, 3001, Australia
[c] Department of Civil Engineering, Abu Dhabi University, Abu Dhabi, United Arab Emirates
[d] School of Computer Science Engineering and Technology, Bennett University, Greater Noida, India
[e] Faculty of Engineering and Information Technology, University of Technology Sydney, Sydney, NSW, 2007, Australia

ARTICLE INFO

Article history:
Received 12 July 2021
Received in revised form
18 October 2021
Accepted 2 December 2021
Available online 28 January 2022

Keywords:
Compression index
Artificial intelligence
Swarm intelligence
Meta-heuristic optimization
Dedicated freight corridor

ABSTRACT

The study proposes an improved Harris hawks optimization (IHHO) algorithm by integrating the standard Harris hawks optimization (HHO) algorithm and mutation-based search mechanism for developing a high-performance machine learning solution for predicting soil compression index. HHO is a newly introduced meta-heuristic optimization algorithm (MOA) used to solve continuous search problems. Compared to the original HHO, the proposed IHHO can evade trapping in local optima, which in turn raises the search capabilities and enhances the search mechanism relying on mutation. Subsequently, a novel meta-heuristic-based soft computing technique called ELM-IHHO was established by integrating IHHO and extreme learning machine (ELM) to estimate soil compression index. A sum of 688 consolidation test data was collected for this purpose from an ongoing dedicated freight corridor railway project. To evaluate the generalization capability of the proposed ELM-IHHO model, a detailed comparison between ELM-IHHO and other well-established MOAs, such as particle swarm optimization, genetic algorithm, and biogeography-based optimization integrated with ELM, was performed. Based on the outcomes, the ELM-IHHO model exhibits superior performance over the other MOAs in predicting soil compression index.

1. Introduction

Considering the rapid industrialization and urbanization in today's modern world, there is a growing demand for solutions to the equally increasing problems in the engineering and construction fields. It is pertinent to mention that the development of a country wholly depends on the availability of infrastructure facilities such as road and railway transportation systems, airports, hospitals, ports, power, etc. These structures are important for faster economic growth and the alleviation of poverty. In the last few decades, we have witnessed a phenomenal change in the development of infrastructure facilities on a fast-track basis, particularly in transportation systems like railways, roadways, airports, metros and flyovers. As we know, all these systems are built on the natural ground surface and during construction, intensive concreting and earthwork are performed. Also, the installation of a transportation system requires substantial investment. Hence, to run the entire system satisfactorily, a detailed analysis of the stability of the structures is extremely needed. Furthermore, proper safety of the structures in terms of defects, seismic failure, malfunction of substructures due to differential settlement of soil layers, etc. should always be ensured during the construction phase and in the post-completion phase as well.

* Corresponding author.
E-mail address: abidhan@nitp.ac.in (A. Bardhan).
Peer review under responsibility of Institute of Rock and Soil Mechanics, Chinese Academy of Sciences.

https://doi.org/10.1016/j.jrmge.2021.12.018

In geotechnical engineering, the design of the sub-structure/foundation is pertinent to determine the compressibility characteristics of soils, such as the compression index (C_c), coefficient of consolidation (C_v), coefficient of compressibility (a_v), and coefficient of volume compressibility (m_v). These values are critical in estimating the settlement of the sub-soils under a given load. In theory, the compressibility of soil is the ease with which a soil decreases in volume (soil densification) when subjected to a load. Reduction of the soil volume mainly occurs due to the drainage of pore water, which is a time-dependent process. For fine-grained and low permeable soils, the settlement estimation depends on the aforementioned parameters, i.e. C_c, C_v, a_v, and m_v. Amongst them, C_c is the main indicator that is often used to calculate the settlement of the foundation in the design phase. However, the accurate estimation of compressibility of soils is an arduous task for fine-grained soils due to their low permeability and the complex process of expulsion of pore water in such types of soils. As mentioned by Li (2014), the estimation of post-construction settlement of sub-soil presents an issue for the serviceability of various structures. In practice, the settlement caused by the increments of loads is derived using e-$\log_{10}\sigma'$ (void ratio versus the logarithm of compressive stress) curve. Subsequently, the amount of total settlement (S_c) for a soil layer of normally consolidated clay (NC-clay) is calculated using the following expression:

$$S_c = H\frac{C_c}{1+e_0}\log_{10}\left(\frac{\sigma'_0+\Delta\sigma}{\sigma'_0}\right) \quad (1)$$

where H is the thickness of the soil layer; e_0 represents the initial void ratio; and σ'_0 and $\Delta\sigma$ are the effective overburden pressure and applied load, respectively. Now, the task at hand is the determination of parameter C_c, which is generally obtained by a standard consolidation test on an undisturbed soil sample collected from sites at different depths in the laboratory. However, this test is time-consuming, cumbersome, and expensive, and usually takes 7 d or more to complete. Therefore, the accurate estimation of C_c would only be possible after a gap of at least 7 d after conducting the test in the laboratory. This test is not only time-consuming and expensive but also requires experienced geotechnical engineers, skilled manpower and specific laboratory equipment to attain reliable results. As mentioned above, estimation of sub-soil settlement is an indirect measure of the stability and reliability of a structure. In fact, C_c is a widely used parameter in the design phases of various structures, including building foundations, bridge piers, retaining walls, railway embankment and foundations of transmission line towers. Keeping these limitations in mind, it is a practical need to establish potential alternative methods to determine soil C_c utilizing its basic physical properties.

Thus, to avoid the operation of conducting actual oedometer test in the laboratory, several studies have been performed to correlate C_c with basic soil properties. Numerous statistical analyses (Skempton and Jones, 1944; Nishida, 1956; Cozzolino, 1961; Terzaghi et al., 1967; Sower and Sower, 1970) were performed using single and multiple regression techniques. However, these techniques present notable modeling drawbacks, and in many cases, satisfactory correlations could not be achieved, according to a careful examination of these empirical models (Mohammadzadeh et al., 2014). Also, due to the heterogenic nature of soils and the uncertainties associated with them, the derived expressions do not have a high degree of precision or a generalized solution. Hence, more robust and accurate methods are required to correlate the soil C_c by utilizing its basic properties.

In order to predict the desired outcome, including real-world engineering issues, modern research has turned to advanced soft computing approaches as feasible alternatives (Gandomi et al., 2013; Kordnaeij et al., 2015; Bui et al., 2018; Acharyya and Dey, 2019; Mirabbasi et al., 2019; Wróbel and Kulawik, 2019; Armaghani and Asteris, 2020; Cai et al., 2020; Golafshani et al., 2020; Nhu et al., 2020; Sharifi et al., 2020; Ly et al., 2021; Mohammed et al., 2021; Wang and Goh, 2021). Soft computing techniques employ nonlinear modelling as a viable approach for simulating numerous complicated geotechnical processes (Zhang and Goh, 2016; Goh et al., 2017, 2018, 2020; Chen et al., 2020; Wang et al., 2020a, b; Zhang et al., 2017, 2019, 2020a, b, 2021a, b), including prediction of soil C_c. In the recent past, extensive researches have been performed to develop several soft computing-based models to predict C_c including artificial neural network (ANN) (Kolay et al., 2011; Park and Lee, 2011; Alam et al., 2014; Kashefipour and Daryaee, 2014; Mohammadzadeh et al., 2014; Kurnaz et al., 2016; Bui et al., 2018; Kurnaz and Kaya, 2018; Alizadeh Majdi et al., 2019; Benbouras et al., 2019), genetic programming-based models (Mohammadzadeh et al., 2014, 2016, 2019; Bui et al., 2018; Benbouras et al., 2019), support vector machine (SVM)-based models (Samui et al., 2011, 2012; Shi and Guo, 2013; Bui et al., 2018; Kurnaz and Kaya, 2018), and extreme learning machine (ELM) (Samui and Kim, 2017; Kurnaz and Kaya, 2018). In addition, Mamudur and Kattamuri (2020) and Bui et al. (2018) used extra gradient boosting (EGB) method and random forest (RF), and Samui and Kim (2017) used minimax probability machine regression (MPMR) model to correlate C_c with basic soil properties and attained significant accuracy. Table 1 presents the details of earlier studies along with the predictive model employed in each study, and accuracies attained in the training and testing phases for the different models. For the works mentioned in Table 1, out of the multiple predictive models, only the models with the highest R^2

Table 1
Previous studies on prediction of C_c of soil for comparison.

Earlier Studies	Model used	Dataset used	R^2	
			Training	Testing
Mohammadzadeh et al. (2014)	ANN	108	0.8705	0.8593
Benbouras et al. (2019)	ANN	373	0.6464	0.5625
Alizadeh Majdi et al. (2019)	ANN	150	0.961	0.958
Park and Lee (2011)	ANN	947	0.896	0.885
Kashefipour and Daryaee (2014)	ANN	137	0.67	0.7
Kurnaz et al. (2016)	ANN	246	0.8926	0.8973
Alam et al. (2014)	ANN	391	0.76	0.72
Kolay et al. (2011)	ANN	700	-	0.5776
Bui et al. (2018)	BP-MLPNN	154	0.935	0.862
Kurnaz and Kaya (2018)	BRNN	351	0.8887	0.9153
Bui et al. (2018)	RBF-NN	154	0.842	0.678
Mohammadzadeh et al. (2019)	GEP	108	0.8231	0.8603
Benbouras et al. (2019)	GP	373	0.6058	0.0574
Bui et al. (2018)	GP	154	0.904	0.797
Mohammadzadeh et al. (2014)	GP-MEP	108	0.8742	0.8118
Mohammadzadeh et al. (2016)	MGGP	108	0.856	0.84
Samui et al. (2011)	LSSVM	257	0.996	0.5329
Samui et al. (2012)	RVM	185	0.9683	0.9216
Kurnaz and Kaya (2018)	SVM	351	0.8761	0.9147
Shi and Guo (2013)	SVM	49	0.9663	0.9448
Bui et al. (2018)	SVR	154	0.881	0.777
Kurnaz and Kaya (2018)	ELM	351	0.8642	0.883
Samui and Kim (2017)	ELM	186	0.9604	0.8649
Mamudur and Kattamuri (2020)	EGB	391	0.985	0.98
Bui et al. (2018)	RF	154	0.99	0.804
Samui and Kim (2017)	MPMR	186	0.992	0.6906

Note: BP-MLPNN – Back-propagation multi-layer perceptron neural network; BRNN – Bayesian regularization neural network; GEP – Gene expression programming; GMDH – Group method of data handling; GP-MEP – GP-based multi-expression programming; GP – Genetic programming; LSSVM – Least-square support vector machine; MGGP – Multi-gene genetic programming; RBF-NN – Radial basis function neural network; RVM – Relevance vector machine; SVR – Support vector regression.

(coefficient of determination) values in the training and testing phases are listed. Detailed review of earlier studies reveals that higher predicative accuracy was usually achieved in the training phase, while reduced accuracy was found (Samui et al., 2011; Samui and Kim, 2017; Bui et al., 2018; Benbouras et al., 2019) in many cases for the testing dataset, which indicates that the developed models were not accurate enough outside the training dataset. The lack of accuracy mainly stems mainly from the black box nature of the algorithm, overfitting issue, multicollinearity, noise in training dataset, etc. Although conventional soft computing techniques provide better accuracy than statistical methods, they only search for a local optimum solution. Therefore, it is necessary to develop models for predicting the desired output with high degree of accuracy in both the training and testing phases. It is also endeavoured to build models where the differences in the accuracies in both the training and testing phases are minimal to ensure the generalization capability as well as robustness of the predictive models.

Many researchers are currently engaged in enhancing the performance of conventional soft computing techniques (such as ANN and adaptive neuro-fuzzy inference system (ANFIS)) by incorporating meta-heuristic optimization algorithms (MOAs) and found notable results. MOAs provide a balanced approach in the exploration and exploitation process, which in turn raises the search capabilities and the performance of the conventional machine learning models. Among the several MOAs, particle swarm optimization (PSO), genetic algorithm (GA), and biography-based optimization (BBO) algorithms have been used extensively in recent time. Several ANN- and ANFIS-based meta-heuristic hybrid models have been developed, including the ANN-PSO (Armaghani et al., 2014; Hajihassani et al., 2014; Hasanipanah et al., 2017; Asmawisham Alel et al., 2018; Bui et al., 2018; Koopialipoor et al., 2019; Le et al., 2019; Moayedi et al., 2020; Roy and Singh, 2020), ANN-GA (Le et al., 2019; Moayedi et al., 2020; Rad et al., 2020), ANN-BBO (Roy and Singh, 2020), ANN-GWO (grey wolf optimization) (Golafshani et al., 2020), ANFIS-PSO (Roy and Singh, 2020; Ly et al., 2021), ANFIS-GA (Ly et al., 2021), ANFIS-BBO (Roy and Singh, 2020; Ly et al., 2021), and ANFIS-GWO (Golafshani et al., 2020) models. By the use of the ANFIS-PSO model, Ly et al. (2021) predicted the load-bearing capacity of concrete-filled steel tubes and concluded that the ANFIS-PSO outperformed the ANFIS-GA and ANFIS-BBO models. Golafshani et al. (2020) used GWO to enhance the performance of classical ANN and ANFIS models and stated that implementation of MOA can reduce the weakness of classical machine learning algorithms. Le et al. (2019) performed a comparative study of ANN-PSO, ANN-GA, ANN-ICA (imperialist competitive algorithm), and ANN-ABC (artificial bee colony). The authors concluded that the ANN-GA outperformed the other models in predicting the heating load of buildings' energy. Bui et al. (2018) proposed a hybrid model of multi-layer perceptron (MLP) neural networks and PSO (PSO-MLP neural networks) to estimate soil C_c. Experimental results demonstrated that the proposed model outperformed the other conventional machine learning models at all levels. Additionally, many other studies used ANN- and ANFIS-based hybrid model to estimate the desired output(s) in different disciplines of civil engineering (Armaghani et al., 2014; Hajihassani et al., 2014; Hasanipanah et al., 2017; Asmawisham Alel et al., 2018; Bui et al., 2018; Golafshani et al., 2020; Koopialipoor et al., 2019; Le et al., 2019; Moayedi et al., 2020; Rad et al., 2020; Roy and Singh, 2020; Ly et al., 2021). However, a thorough examination of these studies indicates that the performance of meta-heuristic hybrid models is problem-specific as most of the authors reported mixed accuracy levels in their studies. Also, the authors used the standard version of MOA to perform the optimization tasks in their respective studies. Nonetheless, as per no free lunch (NFL) theorem (Wolpert and Macready, 1995), no algorithm provides perfect solutions for all optimization problems. Therefore, implementing a standard version of MOA in hybrid modeling does not ensure the optimum hybrid model generation. Researchers reported modified versions of several MOAs and demonstrated that the performance of standard MOA could be improved by implementing different strategies (Jia et al., 2003; Zhou et al., 2009; Farswan et al., 2016; Mittal et al., 2016; Tian and Shi, 2018). However, existing literature does not show sufficient implementation of the enhanced versions of MOAs and comparative assessment of standard and enhanced version of MOA in predicting the desired output in different fields of engineering.

In light of the aforementioned gaps and limitations, the goal of this research was to develop an effective hybrid model for predicting one of the most challenging real-world problems in civil engineering, i.e. estimation of C_c of soils. A recently developed MOA, namely Harris hawks optimization (HHO), was employed by coupling it with ELM, as a novel hybrid meta-heuristic model, i.e. ELM coupled HHO (ELM-HHO) is proposed. ELM is a simple and efficient machine learning technique that mimics the structure of ANN. ELM, on the other hand, operates on a different principle. ELM achieves good generalisation performance with a single layer of hidden neurons while learning at an incredibly fast learning pace (Huang et al., 2006). On the other hand, HHO is a newer (Heidari et al., 2019) MOA, which shadows the behavior of Harris hawk birds in searching for and chasing prey in nature. It is not only fast and powerful (Heidari et al., 2019; Sihwail et al., 2020) but also a high-performance population-based MOA. Based on the experimental outcomes, the founded researches suggest that HHO outperforms other well-established algorithms (such as PSO, GA, BBO, etc.) and has very competitive results. Considering these advantages, HHO was employed in this work to build an efficient computational model for the prediction of C_c of soils.

However, HHO does present some limitations, such as the limited solution in the initialization phase, local minima trapping issue, and premature convergence. The algorithm also depends on the rabbit energy, which starts at 2 and progressively concentrates to 0 with iteration count. Until the rabbit energy is more than 1, this algorithm only does a global search in the first half of iterations, meaning that it does not perform a global search in the second half of iterations. Furthermore, early convergence results in a local solution rather than a global solution (Jia et al., 2019; Ridha et al., 2020). Hence, based on these shortcomings, this study was motivated to improve the standard HHO algorithm by incorporating a mutation-based search technique to sidestep the above-mentioned issues and enhance the performance of the standard HHO algorithm. Afterward, the improved HHO (IHHO) was used to construct the hybrid models of ELM and IHHO (ELM-IHHO) for predicting C_c of soils. Also, to overcome the overfitting and multicollinearity issues, Principal component analysis (PCA) was implemented. Then, the robustness of the proposed ELM-HHO and ELM-IHHO models was compared with three widely used MOAs, i.e. PSO, GA, and BBO, coupled with ELM. A wide range of oedometer test data was acquired for this purpose from an ongoing dedicated freight corridor (DFC) railway project and used in the current study to forecast the C_c values of soils.

The rest of the work is structured as follows. The study area and data collection are presented in Section 2, while the comprehensive methodology is illustrated in Section 3. Section 4 explains data processing, analysis, and performance parameters. Section 5 shows the findings and a detailed discussion on the performance of the constructed hybrid ELMs. Finally, in Section 6, summary and conclusions are presented.

2. Study area and data collection

The Ministry of Indian Railways (MIR) plans to construct a 10,122-km long heavy-haul railway corridor to address the increased demand for railway freight in India, especially for the movement of railway freight (Raghuram and Verma, 2019). The MIR has planned to construct six DFCs under the Golden Quadrilateral Freight Corridor Project. The rail network will join all of the four largest metropolitan cities of Kolkata, Mumbai, Delhi, and Chennai. As of now, two DFCs, i.e. Eastern and Western DFC (EDFC and WDFC), have been planned and are in the construction stage.

In this study, a 308 km long section of WDFC (Iqbalgarh – Vadodara section with a revised length of 340 km) located between latitude 22°14′58.2″N and longitude 73°11′4.9″E and latitude 24°20′47″N and longitude 72°32′2.8″E (see Fig. 1) was selected as the study area. The entire 340-km segment will pass through Gujarat, India. Presently, the work is in progress in the Iqbalgarh – Vadodara section, from which consolidation test results of the subgrade soil have been collected. A sum of 688 odometer tests along with other soil test data, i.e. depth of soil, specific gravity, bulk density, dry density, water content, gravel content, contents of coarse, medium and fine sands, silt and clay content, plasticity characteristics, and the free swell index has been collected from the project site of Iqbalgarh – Vadodara section and used in this study for predicting soil C_c.

3. Methodology

In this section, the methodological development of the ELM model along with the methodologies of PSO, GA, BBO, and HHO is discussed. This is followed by the methodological development of the IHHO algorithm with ELM-based MOAs in optimizing the weights and biases of ELM. Before the discussion of ELM and MOAs, the theoretical background of the PCA is described.

3.1. PCA

PCA is a common technique to derive characteristics as well as for the dimension reduction of data (Nhu et al., 2020). This technique is well-known for obtaining smaller numbers of uncorrelated elements from more extended predictor variables. To do so, eigenvectors are calculated from the covariance matrix. For a set of p dimensional predictor variable:

$$\boldsymbol{u}_i = [u_i(1), u_i(2), u_i(3), \ldots, u_i(p)]^{\mathrm{T}} \ (i = 1, 2, \ldots, q) \tag{2}$$

PCA transforms it into a new vector $\boldsymbol{v}_i$ which is presented as follows:

$$\boldsymbol{v}_i = \boldsymbol{U}^{\mathrm{T}}\boldsymbol{u}_i \tag{3}$$

where $\boldsymbol{U}$ stands for the $p \times p$ orthogonal matrix whose jth column $\boldsymbol{c}_j$ represents the jth eigenvector of the example covariance matrix $\boldsymbol{M}$ given by

$$\boldsymbol{M} = \frac{1}{q}\sum_{i=1}^{q}\boldsymbol{u}_i\boldsymbol{u}_i^{\mathrm{T}} \tag{4}$$

The solution of PCA is given by

$$\lambda_i\boldsymbol{r}_j = \boldsymbol{M}\boldsymbol{r}_j \ (j = 1, 2, \ldots, p) \tag{5}$$

where λ_i stands for an eigenvalue of the covariance matrix ($\boldsymbol{M}$), and $\boldsymbol{r}_j$ shows the corresponding eigenvector. In Eq. (3), the orthogonal element of the predictor variable $\boldsymbol{v}_i$ can be calculated by changing $\boldsymbol{u}_i$, where the principal component stands for the resultant part. At first, the eigenvalues sort the eigenvector from high to low and then choose the main element. In turn, the predictor variable causes the reduction of the main component. PCA is used to reduce the dimensions of various variables down to the main element so that they are not related and their variance is at a continuous maximum.

3.2. Details of soft computing techniques

3.2.1. ELM

ELM is a single-layer feed-forward network (SLFNN) that uses a closed-form solution to generate weights through a least-squares method. A continuous probability distribution function is also used rather than an iterative method of conventional feed-forward ANNs. The strengths of ELM include design simplicity, high speed of

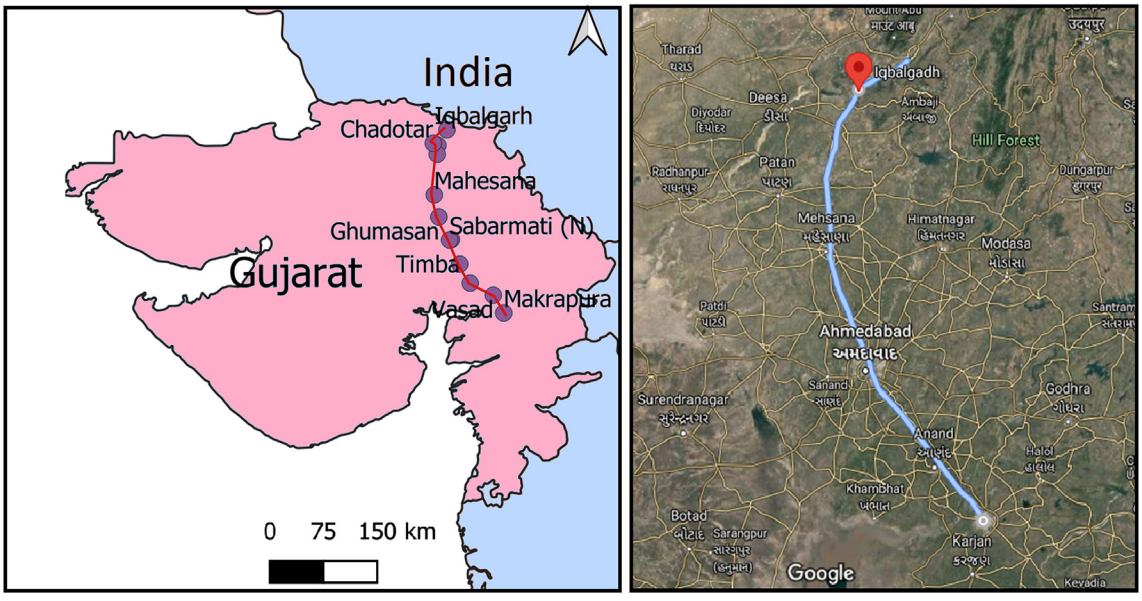

Fig. 1. Geographical layout of Iqbalgarh – Vadodara section.

solving regression or classification problems associated with the randomized nature of the bias and weights in hidden neurons, and the uniqueness of the least-square solution of the output obtained using the Moore-Penrose pseudo inverse. These properties obviate the requirement for an iterative training technique, such as ANN-based models, which are vulnerable to being trapped in local minimums in predictor datasets.

The steps to construct the procedure for data modelling based on ELM include: (i) randomly constructing the weights and biases of the hidden layer neurons in contrast to the iterative method used in ANNs; (ii) assembling the hidden layer's weights by progressing the inputs through the hidden layer's parameters; and (iii) estimating output weights through matrix operations, where the generalized Moore-Penrose inverse matrix is utilized followed by calculating its product with the response variable, i.e. solving a collection of linear equations. After hidden neuron nodes are identified, they must undergo randomization. Hidden neurons can be normally detected by trial-and-error approaches. The benefits of ELM compared to other models in real-time applications include high convergence rate, great potential for generalizability, not being trapped in local minimal solutions, no data overfitting, and no need for iterative tuning. In addition, the high-speed and promoted performance of ELM is highly beneficial, especially in a real-time setting.

ELM is generally used to train the predictor-target pairs of data in the present study, as shown in Fig. 2. Let x_i denote the predictors and y_i be the target. The following mathematical representation was used for the SLFNN with L hidden neurons for a collection of d-dimensional vectors defined with i ($i = 1, 2, \ldots, N$) training samples:

$$f_L(x) = \sum_{i=1}^{L} h_i(x)\beta_i = \boldsymbol{h}(x)\boldsymbol{\beta} \tag{6}$$

where $h_i(x)$ represents the ith hidden neuron; $\boldsymbol{\beta} = [\beta_1, \beta_2, \ldots, \beta_L]^{\mathrm{T}}$ is the output weight matrix between the hidden and output neurons; and $\boldsymbol{h}(x) = [h_1, h_2, \ldots, h_L]$ is the hidden neuron output that shows the hidden randomised properties of the predictor x_i. The following equation was used to express the output function of hidden neurons:

$$h_i(x) = G(a_i, b_i, x)\left(a_i \in \boldsymbol{R}^{\mathrm{d}}, b_i \in \boldsymbol{R}\right) \tag{7}$$

where $G(a_i, b_i, x)$ is defined as a piecewise continuous nonlinear function using hidden neuron parameters (a_i and b_i) that is required to meet the ELM approximation theorem. The commonly used sigmoid equation in ANN-based models was employed to develop the ELM model as follows:

$$G(a, b, x) = \frac{1}{1 + \exp(-ax + b)} \tag{8}$$

Huang et al. (2006) minimized the estimation error by employing least-square fitting when deriving the weights linking output and hidden layers:

$$\min_{\beta \in \boldsymbol{R}^{L \times m}} ||\boldsymbol{H}\boldsymbol{\beta} - \boldsymbol{T}||^2 \tag{9}$$

where $||\boldsymbol{H}\boldsymbol{\beta} - \boldsymbol{T}||$ represents the Frobenius norm; and $\boldsymbol{H}$ is a randomized hidden layer output matrix and defined as

$$\boldsymbol{H} = \begin{bmatrix} \boldsymbol{g}(x_1) \\ \vdots \\ \boldsymbol{g}(x_N) \end{bmatrix} = \begin{bmatrix} g_1(a_1x_1 + b_1) & \cdots & g_L(a_Lx_1 + b_L) \\ \vdots & \ddots & \vdots \\ g_1(a_Nx_N + b_1) & \cdots & g_L(a_Lx_N + b_L) \end{bmatrix} \tag{10}$$

The following target matrix is used during the data training:

$$\boldsymbol{T} = \begin{bmatrix} \boldsymbol{t}_1^{\mathrm{T}} \\ \vdots \\ \boldsymbol{t}_N^{\mathrm{T}} \end{bmatrix} = \begin{bmatrix} t_{11} & \cdots & t_{1m} \\ \vdots & \ddots & \vdots \\ t_{N1} & \cdots & t_{Nm} \end{bmatrix} \tag{11}$$

The linear equation system $\boldsymbol{\beta}^* = H^+\boldsymbol{T}$ was solved to obtain an optimal solution, in which H^+ represents the generalized Moore-Penrose inverse function. Moreover, the optimal solution was inserted into this equation to make predictions for x as a given input vector.

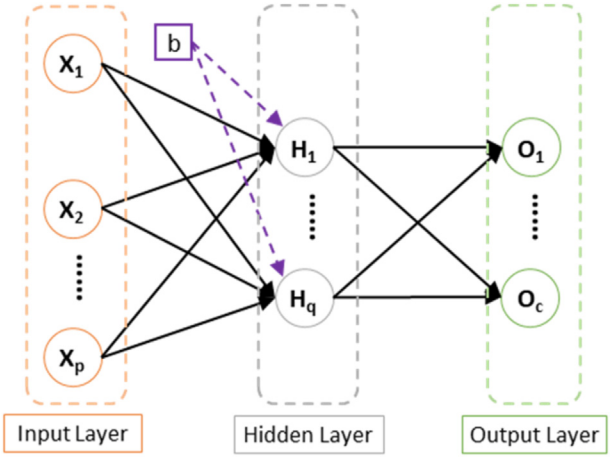

Fig. 2. A general structure of ELM.

3.2.2. PSO

The PSO is considered the first of the segment of the swarm-based MOA (Kennedy and Eberhart, 1995). The principal origin of impulse for the PSO algorithm is to gather and school patterns among birds and fish, so that the central goal of this algorithm is to provide a universal best resolution in multidimensional space. The PSO initializes the particle's random speeds and status. After updating the situation, every particle based on the rates identifies the best position in the multidimensional period for the individual and the global most suitable positions. The universal most suitable status is regarded as the best positions in every particle and the best status of a particle stands for the most suitable state. The individual most suitable position and the direction of the global most suitable state play a role in the updating process of a particle. The distinction between the universal most suitable state and their individual most suitable position is critical to update the particle speed. As shown in Fig. 3, one can observe that through a blend of exploitation and investigation during k and $k+1$ iterations, the particles gather everywhere around the best resolution:

$$v_{\mathrm{i}}^{k+1} = \omega v_{\mathrm{i}}^{k} + c_1 r_1 \left(pbest_i - x_{\mathrm{i}}^{k}\right) + c_2 r_2 \left(gbest_i - x_{\mathrm{i}}^{k}\right) \tag{12}$$

$$x_{\mathrm{i}}^{k+1} = x_{\mathrm{i}}^{k} + v_{\mathrm{i}}^{k+1} \tag{13}$$

where x and v stand for the position and velocity, respectively; *pbest* and *gbest* represent the best particle position and best group position, respectively; r_1 and r_2 are the random numbers between 0 and 1; and c_1 and c_2 are the cognitive and social coefficients. These parameters are problem-oriented; thus, their main goal is to distinguish the level of reliance of a particle upon its personal and global positions. ω stands for the inertia weight parameter, which has a direct relation with the time:

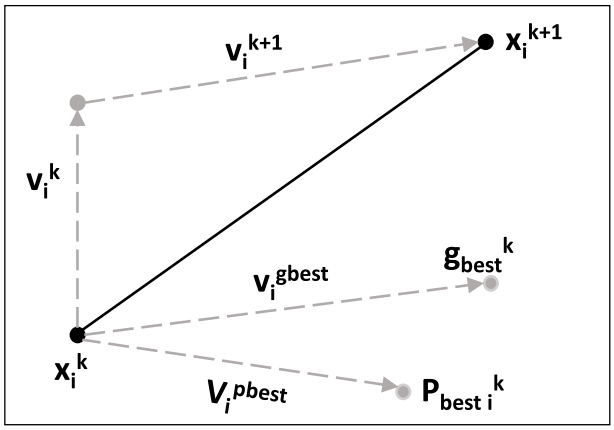

Fig. 3. Movement of *i*th particle in the search space during *k* and *k*+ 1 iterations.

$$\omega^k = \omega_{max} - \frac{\omega_{max} - \omega_{min}}{k_{max}} k \tag{14}$$

where ω_{min} and ω_{max} are the minimum and maximum inertia weights, respectively; and k_{max} is determined according to the highest number of iterations. Similar to GA, particles in the PSO do not bid against each other, rather they support. The number of particles in PSO is an important characteristic of the model, differentiating it from other optimization approaches, which allows the identification of global optima. The detailed steps involved in PSO are presented in the flowchart in Fig. 4.

3.2.3. GA

The biological evolution of human beings can be thought of as a GA in the sense that optimal results, or the fittest human, are the desired output. In 1992, Holland (1992) used GA in various applications and achieved significant results. Combining the correct responses in the GA, in correlation with the survival of the strongest of evolution, leads to an optimized resolution. In each step, selected chromosomes from present populations are used to construct the next generation by employing three types of genetic operators, namely selection, crossover, and mutation.

The selector operator initially selects a generation to participate in the reproduction process based on fitness parameters, which are heavily influenced by the presence or absence of a chromosome. Then, the crossover operator randomly selects a locus between two chromosomes, whereby the crossover suggests different solutions for the present population. The range of the crossover point varies from 1 to $\min(LA^{P_1}, LA^{P_2}) - 1$, where LA^{P_1} and LA^{P_2} are the numbers of location areas in parent resolutions P_1 and P_2, respectively. The re-permutation in the sequence of the bits in chromosomes does not affect the topology but does change the placements. These three processes (i.e. selection, crossover, and mutation) continue until the terminating criterion is reached. These criteria include the number of iterations, number of generations, changes in fitness, etc., which are important in GA. In each iteration, each individual is assessed based on fitness. The most fitted generation with the least fitness value is considered in the developed model. The typical flowchart of GA in Fig. 5 shows the steps along with different genetic operators and their operations.

3.2.4. BBO

The BBO algorithm, first suggested by Simon (2008), was motivated by biogeography, or the development of steady ecosystems containing different species and the impacts of immigration and emigration. The study used this algorithm to investigate the biological organisms regarding geographical patterns (over time and space) of various landscapes, islands, and continents over decades or even millennia. Specifically, the migration and mutation between the diverse species of many different ecosystems and habitats were investigated. The principal characteristic of BBO is defined as the migration from high to low characteristics and the mutation of low characteristics to high. Repeating this procedure led to an optimized resolution, where some descriptions of migration and mutation were employed as the base operators of the above algorithm.

(1) Migration. In this case, the operator transfers data between resolutions. The movement and migration parameters below specify this parameter:

$$\lambda_k = \lambda_{max}\left(1 - \frac{k}{k_{max}}\right) \tag{15}$$

$$\mu_k = \mu_{max}\frac{k}{k_{max}} \tag{16}$$

where λ_k is the immigration rate, μ_k is the emigration rate, and k stands for the rank of resolution. Here, for the largest number of species (S_{max}), we obtained identical rates of immigration and

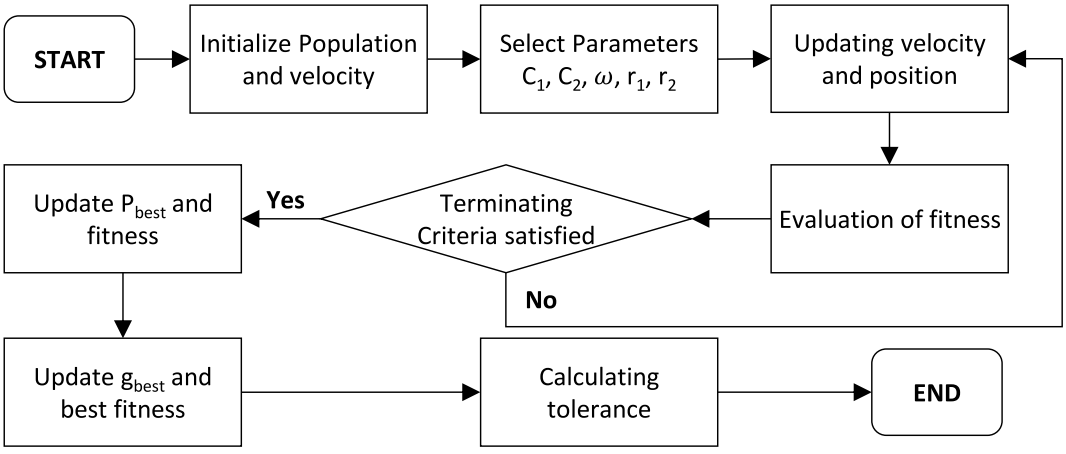

Fig. 4. Steps showing the process involved in PSO.

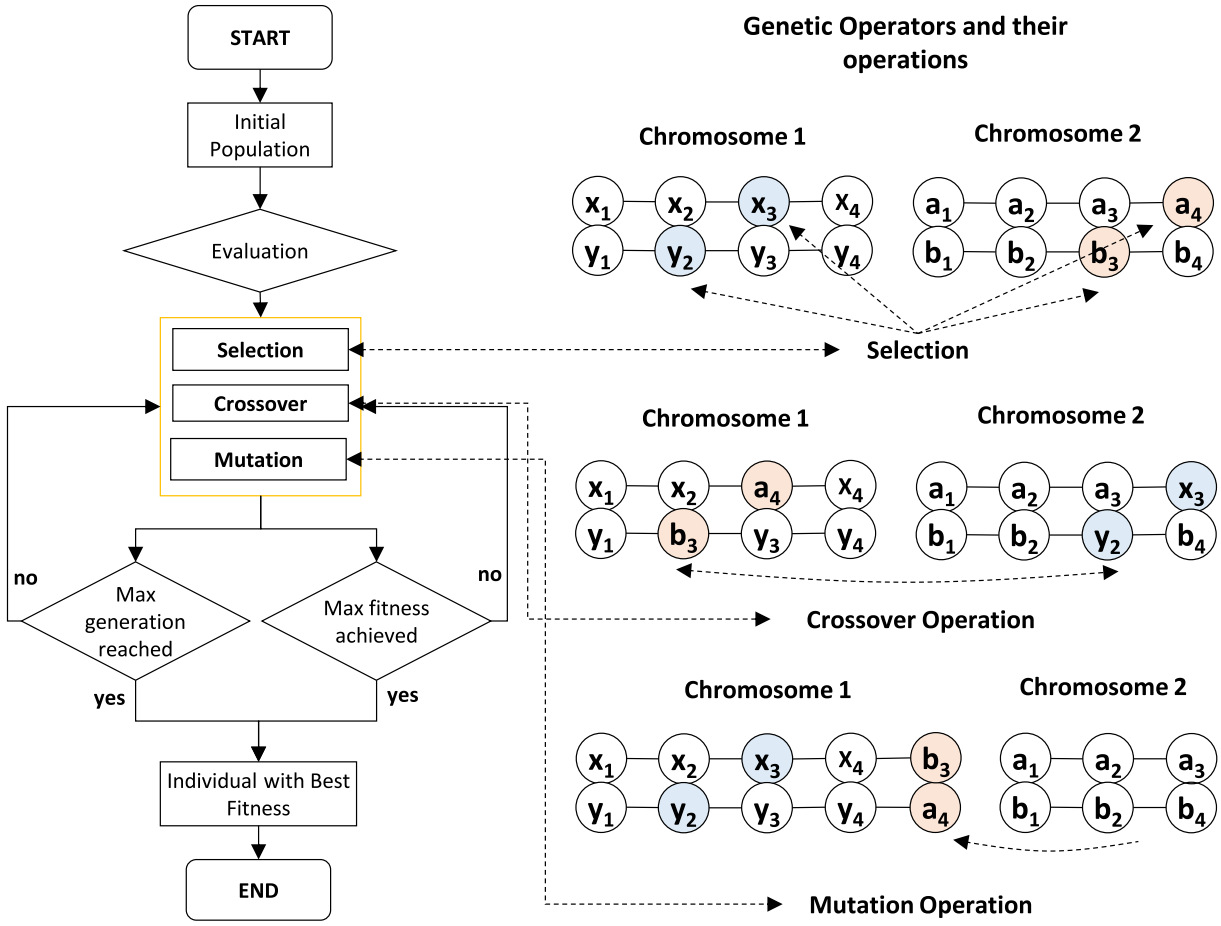

Fig. 5. Flowchart of GA.

emigration. Fig. 6 shows the relationship between emigration rate and immigration rate in BBO.

(2) Mutation. Since catastrophes or infections change the coefficients of the resolution, the sudden change in species shows the notion of mutation. The calculation of transformation among species is as follows:

$$m_k = m_{\max}\left(1 - \frac{P_k}{P_{\max}}\right) \tag{17}$$

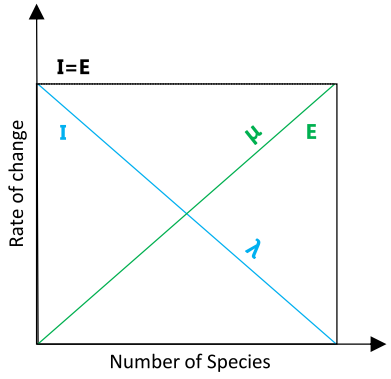

Fig. 6. Relationship between emigration rate and immigration rate.

where m_k and $m_{\max}$ are the representative transformation rates; and P_k and $P_{\max}$ are the possible species, in which k shows the rank of resolution. P_k is expressed as follows:

$$P_k = \begin{cases} -(\lambda_k + \mu_k)P_k + \mu_{k+1}P_{k+1} & (k = 0) \\ -(\lambda_k + \mu_k)P_k + \lambda_{k-1}P_{k-1} + \mu_{k+1}P_{k+1} & (1 \le k \le k_{\max} - 1) \\ -(\lambda_k + \mu_k)P_k + \lambda_{k-1}P_{k-1} & (k = k_{\max}) \end{cases} \tag{18}$$

Previous reports on the application of this meta-heuristic algorithm in predicting real-world problems (Zheng et al., 2016; Roy et al., 2021) indicate that this optimization algorithm can enhance the performance of conventional machine learning models with significant success. However, a typical flowchart of BBO in presented in Fig. 7.

3.2.5. HHO

Heidari et al. (2019) introduced the HHO as a novel optimization algorithm based on the teamwork among hawks in pursuing the prey, which was motivated by the natural behavior of Harris's hawk. In HHO, a group of hawks attempts to take an identified prey by surprise through collaboratively striking from different directions and simultaneously converging on it. Harris's hawks employ a variety of pursuit strategies according to the circumstances and the prey's escape patterns. As the best hawk, the leader of the group abruptly disappears from sight after attacking and following the prey for a while. The next member of the group then carries on the chase. The exhausted and vulnerable prey can be ultimately hunted using this switching tactic. Applicability to

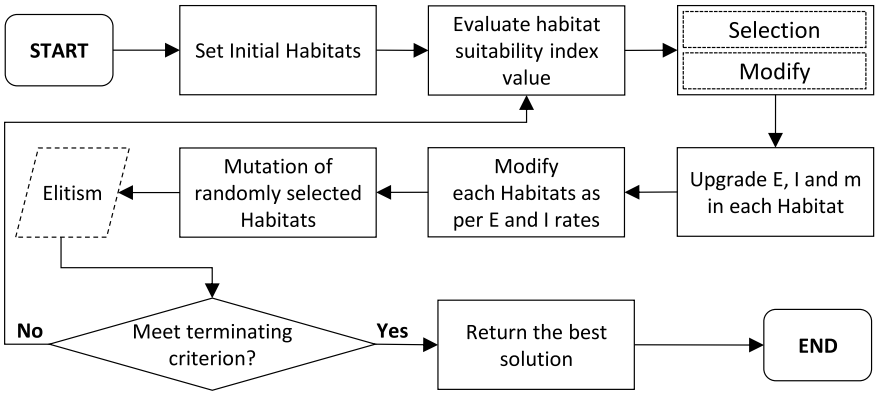

Fig. 7. Flowchart showing the steps of BBO.

constrained problems constitutes a strength of the HHO algorithm. The HHO, as a global optimizer, may also establish a balance between the exploitation and exploration stages. The HHO is comprised of three main phases. The first phase to model the exploration is as follows:

$$x(t+1)=\begin{cases} x_{\text{rand}}(t)-r_1|x_{\text{rand}}(t)-2r_2x(t)| & (q\geq 0.5)\\ x_{\text{rabbit}}(t)-x_{\text{m}}(t)-r_3[LB+r_4(UB-LB)] & (q<0.5)\end{cases} \tag{19}$$

where $x(t)$ and $x(t+1)$ are the current and next iterations, respectively; $x_{\text{rand}}(t)$ represents a randomly selected hawk from the present population; $x_{\text{rabbit}}(t)$ is the prey's position; r_1, r_2, r_3, r_4 and q are uniformly distributed in [0, 1]; UB and LB are the upper and lower bounds, respectively; and x_{m} describes the average location of the hawks as follows:

$$x_{\text{m}}(t)=\frac{1}{N}\sum_{i=1}^{N}x_i(t) \tag{20}$$

where $x_i(t)$ is the location of each hawk in the tth iteration, and N is the total number of hawks. Moreover, the transition between the exploration and exploitation constitutes the next (second) phase of the algorithm. The prey's energy is modeled using the following equation, which continuously decreases due to the chasing and escaping behavior:

$$E=2E_0\left(1-\frac{t}{T}\right) \tag{21}$$

where E_0 is the prey's initial energy, T represents the maximum iteration number, and E is its escape energy. In each iteration of the HHO algorithm, E_0 can be randomly altered in the range of $[-1, 1]$. Accordingly, the exploitation is performed when $|E|<1$ and the exploration occurs when $|E|\geq 1$, and the exploitation constitutes the final (third) phase that primarily seeks to derive a local solution from previously obtained solutions. In the final phase, hawks perform the surprise attack and strike the prey that was identified in the previous phase. In summary, the following four strategies are presented to model the attacking phase based on the hawks' chasing model and the prey's escaping behavior:

(1) Soft besiege. Soft besiege occurs when the prey has sufficient energy and hawks are trying to make the prey tired. If the prey successfully escapes as shown by r, this strategy can be valid for $|E|\geq 0.5$ and $r\geq 0.5$, and can be modeled according as

$$x(t+1)=\Delta x(t)-E|Jx_{\text{rabbit}}(t)-x(t)| \tag{22}$$

$$\Delta x(t)=x_{\text{rabbit}}(t)-x(t) \tag{23}$$

where $J=2(1-r_5)$ is the prey's jump strength, in which r_5 denotes a uniformly distributed number in [0, 1]; and $\Delta x(t)$ is the difference between the locations of the prey and hawk in the tth iteration.

(2) Hard besiege. This strategy is taken when the prey is exhausted with inadequate energy ($r\geq 0.5$ and $|E|<0.5$) and is represented as

$$x(t+1)=x_{\text{rabbit}}(t)-E_{\text{n}}|\Delta x(t)| \tag{24}$$

(3) Soft besiege. This is coupled with a progressive rapid dive by the hawks and occurs when the prey's energy is still for $r<0.5$ and $|E|\geq 0.5$, and the hawks determine the next move, which is described by the following equations:

$$x=x_{\text{rabbit}}(t)-E|Jx_{\text{rabbit}}(t)-x(t)| \tag{25}$$

$$\boldsymbol{Z}=\boldsymbol{Y}+S+LF(D) \tag{26}$$

where D denotes the dimension, LF is the levy flight function, and $\boldsymbol{Z}$ is a $1\times D$ random vector. The following model was therefore used to update the hawks' positions:

$$x(t+1)=\begin{cases}\boldsymbol{Y} & (f(\boldsymbol{Y})<f(y(t)))\\ \boldsymbol{Z} & (f(\boldsymbol{Z})<f(y(t)))\end{cases} \tag{27}$$

(4) Hard besiege. This is coupled with a progressive and rapid dive and is valid when $|E|<0.5$ and $r<0.5$, as described by the following equation:

$$\begin{aligned}&x(t+1)=\{x_{\text{rabbit}}(t)-\\ &E|Jx_{\text{rabbit}}(t)-x_{\text{m}}(t)| \quad (f(\boldsymbol{Y})<f(y(t)))\\ &\{\boldsymbol{Z}=\boldsymbol{Y}+S+LF(D) \quad (f(\boldsymbol{Z})<f(y(t))\end{aligned} \tag{28}$$

The different phases of the HHO proposed by Heidari et al. (2019) are shown in Fig. 8, and the detailed process of HHO is presented in Fig. 9.

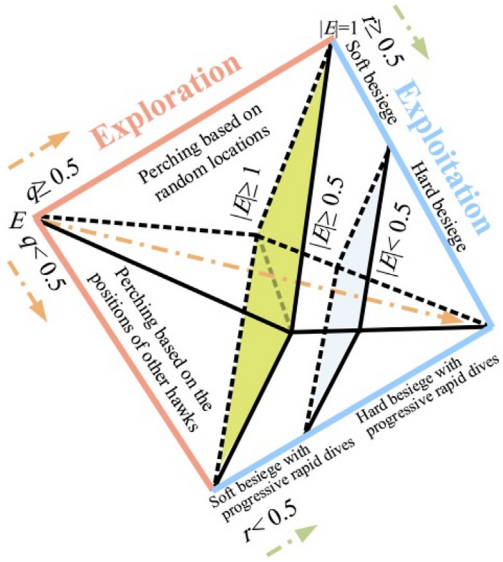

Fig. 8. Different phases of HHO (Heidari et al., 2019).

3.2.6. IHHO

HHO is typically a robust and high-performance MOA used to solve real-world engineering problems. However, according to the NFL theorem, no algorithm delivers perfect solutions to all optimization problems (Wolpert and Macready, 1995). Thus, in order to avoid the limitations of the HHO algorithm and to enhance its capabilities in handling real-world engineering problems, a mutation-based process is incorporated to construct the IHHO. To augment the algorithm's local and global search abilities, a mutation-based mechanism was incorporated to update the current position of each rabbit by generating diverse solution spaces in each iteration. For this, PSO velocity was used, which can be expressed as

$$v_{m+1} = wv_m \tag{29}$$

where w represents the inertia weight; and v_m and v_{m+1} are the velocity of mutants in m and $m+1$ iterations, respectively. In each iteration, the velocity of mutants is updated using the expression given in Eq. (29). Subsequently, the updated velocity is utilized to upgrade the position of the best rabbit using the following expression:

$$X_{\text{rabbit}} = X_{\text{rabbit}} + v_{m+1} \tag{30}$$

If the fitness of the new location is better than that of the present rabbit location, the new position is set as a possible location and the mutation approach is used to improve its location. Subsequently, the best rabbit location is set as the potential rabbit location. In the next iteration, the locations of the current and potential rabbits are compared to select the best location. The entire process of IHHO is given in the form of a pseudo-code in the Appendix.

3.2.7. Hybridization of ELM and MOAs

Several studies have been performed in engineering applications to improve the performance of traditional machine learning models, such as ANN, ANFIS, etc. by integrating MOAs (Koopialipoor et al., 2019; Le et al., 2019; Cai et al., 2020; Golafshani et al., 2020; Roy and Singh, 2020; Ly et al., 2021; Roy et al., 2021). It is pertinent to mention that most real-time data do not follow any specific rules or distributions; rather, they are primarily nonlinear in nature with mixed noise. Hence, it is difficult to handle real-time data for constructing predictive models by utilizing classical machine learning models. In particular, the weakness in finding the exact global minima affects the performance of the classical machine learning models (Bui et al., 2018; Cai et al., 2020; Golafshani et al., 2020), which yield undesirable results and overfitting issues in predicting a new set of data. Also, the local minima trapping issue of ANN leads to erroneous results. Therefore, to sidestep these issues, researchers prepare hybrid models by integrating MOAs with traditional machine learning models to search for the exact global minimum instead of local minima by updating their learning parameters.

In ELM, the learning parameters such as hidden weights and biases are randomly initialized, which may also yield undesirable and inefficient performance due to local minima trapping issues. To alleviate this issue, MOAs can be integrated for finding the exact global minimum. In the present study, the recently proposed HHO algorithm has been utilized to optimize ELM's learning parameters. The methodological development of the hybrid model of ELM and HHO (ELM-HHO) algorithm can be described as follows. The initial stage requires choosing the parametric setting (i.e. number of hidden neurons) and random generation of weights and biases. This is followed by the generation of optimized weights and biases through HHO. Finally, the HHO optimized weights and biases are used for validating the model. To obtain the optimum weights and biases for the remaining hybrid models, including ELM-IHHO, the

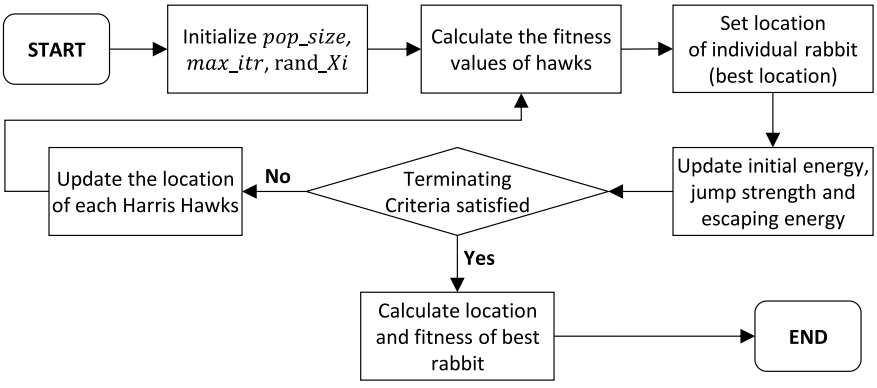

Fig. 9. Flowchart of HHO.

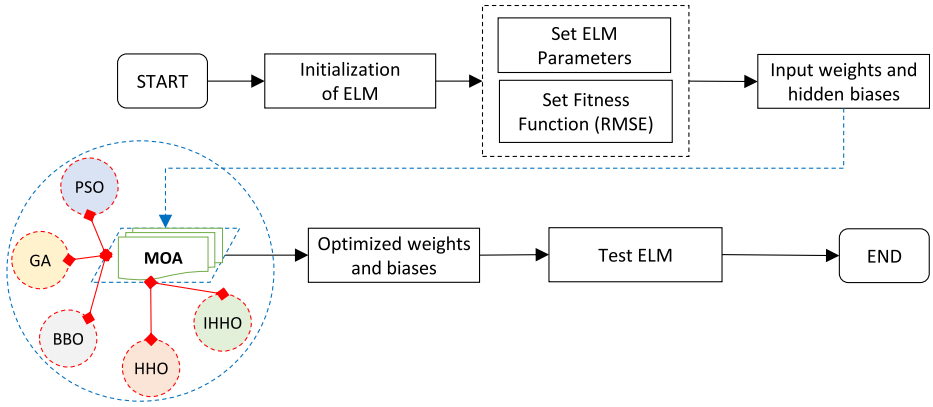

Fig. 10. Steps for constructing hybrid ELMs.

same technique was used. However, the parametric configuration of MOAs (HHO, IHHO, PSO, GA, and BBO) is tuned in each stage, the details of which are given in the results and discussion section. The hybridization process presented in Fig. 10 shows the steps for developing hybrid ELMs in the present study.

4. Processing and analysis of data

4.1. Data preparation

To develop the predictive model for the compression index of soil, consolidation test data containing 688 experimental test records were obtained from an ongoing project site of WDFC. The collected dataset contained information about the depth of soil (*D*), specific gravity (*Gs*), bulk density (*BD*), dry density (*DD*), water content (*WC*), gravel content (*G*), coarse sand content (*CS*), medium sand content (*MS*), fine sand content (*FS*), silt and clay content (*MC*), liquid limit (*LL*), plastic limit (*PL*), free swell index (*FSI*) and compression index (C_c) of different types of soils classified as CI (inorganic clay with intermediate plasticity), CL (inorganic clay with low plasticity), ML (low plasticity silt), ML-CL (clayey silt with low plasticity), SC (clayey sand), and SM-SC (silty sand with clayey sand), respectively. The statistical description of soil parameters is provided in Table 2, specifying the minimum (Min), average (Avg), and maximum (Max) values separately for each type of soil. In total, there are 204 CI soils, 418 CL soils, 2 ML soils, 3 ML-CL soils, 45 SC

Table 2
Statistical summary of the input soil parameters (as per soil types).

Soil	Parameters	*D* (m)	*Gs*	*BD* (g/cm^3)	*DD* (g/cm^3)	*WC* (%)	*G* (%)	*CS* (%)	*MS* (%)	*FS* (%)	*MC* (%)	*LL* (%)	*PL* (%)	*FSI* (%)	C_c
CI (204 soils)	Min	1	2.65	1.66	1.48	10.07	0	0	0	1	52	35	15	10	0.07
	Avg	9.2	2.68	1.82	1.58	14.74	3.46	2.16	3.49	18.18	72.73	38.08	19.72	22.46	0.125
	Max	32.75	2.7	1.98	1.71	24.67	17	11	15	44	97	49	26	73	0.1622
CL (418 soils)	Min	1.00	2.64	1.61	1.46	8.1	0	0	0	3	50	25	12	7	0.062
	Avg	6.29	2.67	1.79	1.59	12.94	2.96	1.95	3.83	27.06	64.2	31.14	18.12	17.68	0.1183
	Max	23.75	2.69	1.99	1.7	21.04	18	10	25	48	97	42	22	35	0.1676
ML (2 soils)	Min	5.75	2.65	1.82	1.65	10.35	4	2	3	11	78	31	23	8	0.1008
	Avg	7.25	2.65	1.84	1.65	11.11	4.5	2	3.5	11.5	78.5	31.5	23.5	8	0.1008
	Max	8.75	2.65	1.85	1.65	11.87	5	2	4	12	79	32	24	8	0.1008
ML-CL (3 soils)	Min	5.75	2.65	1.77	1.62	9.29	1	4	3	31	54	26	19	7	0.094
	Avg	9.75	2.65	1.84	1.65	11.56	1.67	4.33	4	34	56	26.67	19.67	7.33	0.1025
	Max	14.75	2.66	1.94	1.68	15.35	2	5	5	37	58	27	20	8	0.1097
SC (45 soils)	Min	1	2.64	1.61	1.46	8.36	0	0	0	24	36	25	17	7	0.094
	Avg	7.78	2.66	1.78	1.59	12	5.36	2.4	4.38	43.31	44.56	28.4	19.29	11.60	0.1209
	Max	23.75	2.67	1.94	1.68	17.2	17	8	15	62	49	31	21	18	0.1656
SM-SC (16 soils)	Min	1	2.64	1.65	1.5	7.45	0	0	0	38	28	23	17	7	0.1038
	Avg	4.41	2.65	1.74	1.58	9.93	2.5	1.81	4.06	50	41.63	25.69	18.88	10.81	0.1232
	Max	8.75	2.65	1.82	1.64	15.67	12	8	20	59	49	28	21	29	0.149

Table 3
Values of coefficient of correlation between soil parameters and C_c.

Soils	*D*	*Gs*	*BD*	*DD*	*WC*	*G*	*CS*	*MS*	*FS*	*MC*	*LL*	*PL*	*FSI*	C_c
All soils	-0.1	0.08	-0.66	-0.89	-0.07	-0.09	-0.18	-0.3	0.19	-0.06	0.09	0.48	-0.05	1
CI	-0.18	0.09	-0.7	-0.91	-0.12	-0.18	-0.23	-0.29	0.06	0.14	-0.04	0.19	0.01	1
CL	-0.06	-0.02	-0.7	-0.89	-0.11	-0.01	-0.15	-0.31	0.35	-0.24	-0.03	0.63	-0.22	1
ML	-	-	-	-	-	-	-	-	-	-	-	-	-	-
ML-CL	-1	-0.93	-0.98	-1	-0.96	-0.14	0.79	0.62	-0.99	0.99	0.93	0.93	-0.93	1
SC	-0.73	-0.25	-0.88	-0.99	-0.39	-0.57	-0.38	-0.36	0.59	-0.33	-0.23	-0.11	0.44	1
SM-SC	-0.18	-0.34	-0.66	-0.99	0.33	-0.2	-0.33	0.05	0.19	-0.04	0.13	-0.01	0.01	1

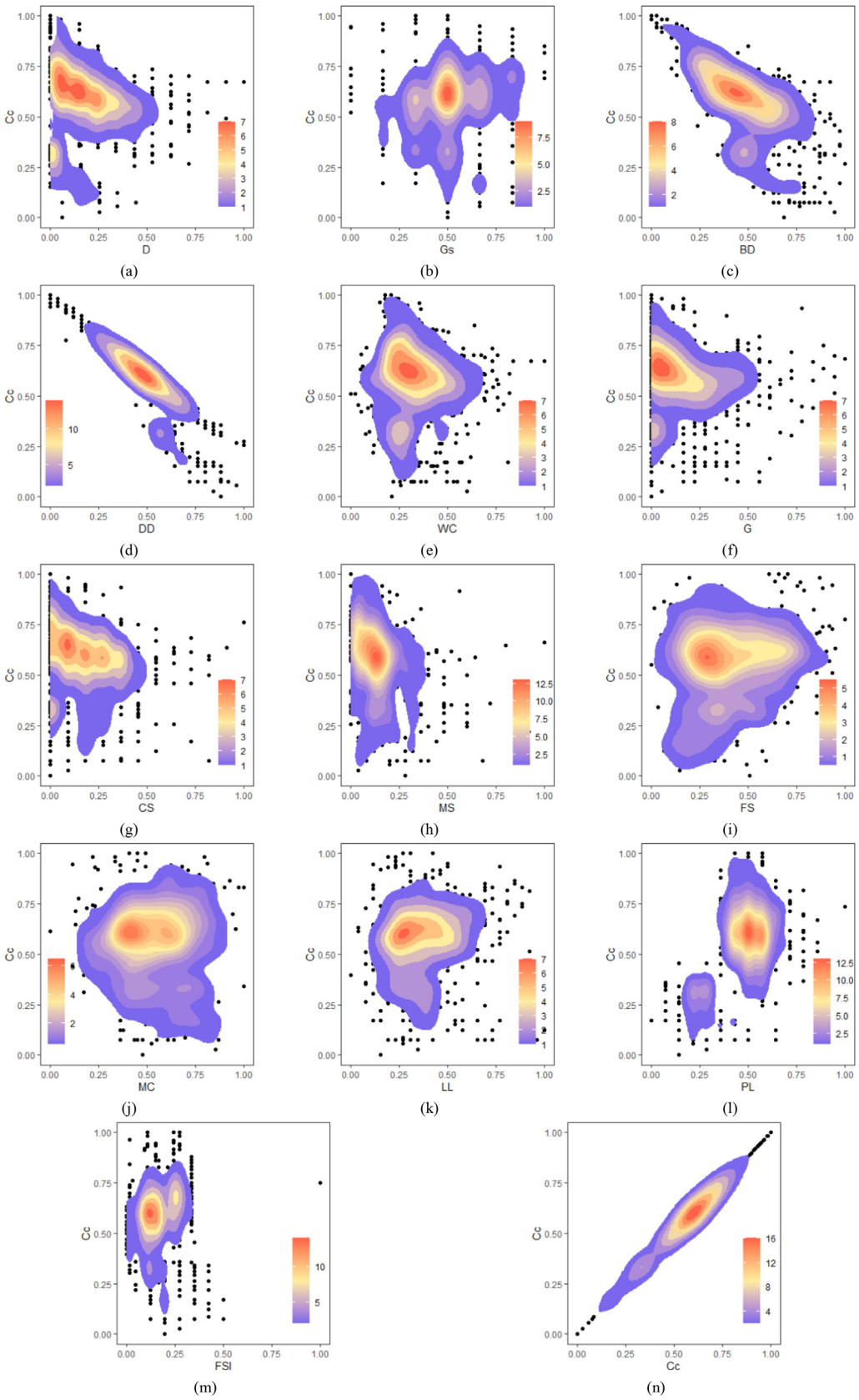

Fig. 11. 2D scatter density plots of (a) *D* vs. C_c, (b) *Gs* vs. C_c, (c) *BD* vs. C_c, (d) *DD* vs. C_c, (e) *WC* vs. C_c, (f) *G* vs. C_c, (g) *CS* vs. C_c, (h) *MS* vs. C_c, (i) *FS* vs. C_c, (j) *MC* vs. C_c, (k) *LL* vs. C_c, (l) *PL* vs. C_c, (m) *FSI* vs. C_c, and (n) C_c vs. C_c. Values are in normalized form.

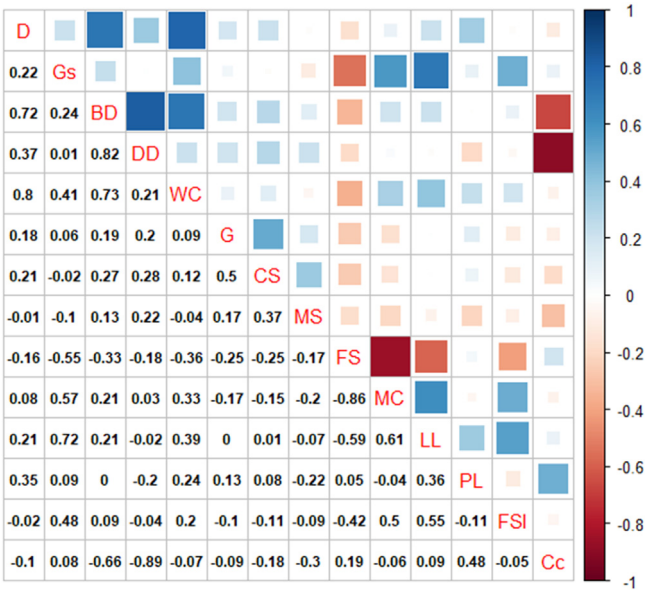

Fig. 12. Correlation matrix.

soils, and 16 SM-SC soils. As can be seen, the C_c value of soil ranges from 0.062 to 0.1676, which indicates that the experimental database contains a wide range of oedometer test results. However, for more clarity, detailed information pertaining to each soil parameters is presented in Table 2.

4.2. Statistical analysis

In this sub-section, the C_c values are correlated with the basic soil properties, i.e. *D*, *Gs*, *BD*, *DD*, *WC*, *G*, *CS*, *MS*, *FS*, *MC*, *LL*, *PL* and *FSI*, the details of which are presented in Table 3. It can be observed that the degree of correlation between C_c and other soil parameters is smaller when all soils are considered. The degree of correlation for CI, CL, SC, and SM-SC soils also small, while no correlation was observed between C_c and ML soil parameters. This suggests that the experimental dataset contained a diverse assortment of uncorrelated data. However, a higher correlation was observed between C_c and *BD* and *DD* in each case. Also, the parameters of ML-CL soil show higher correlations with C_c. The entire descriptive statistics are presented in Table 3 and the details of the collected dataset are presented in the form of a two-dimensional (2D) scatter density plot (Fig. 11) and correlation matrix (Fig. 12) below.

4.3. Dimension reduction using PCA

The experimental high-dimensional dataset was comprised of 13 soil parameters of 688 observations. The degree of correlation between the attributes was found to be on the lower side in many cases. Therefore, to handle the dimensionality effect, PCA was implemented in this study to reduce the number of input variables and dimensionality effect through principal components (PCs). To predict the desired output, PCA generates a new combination of PCs, i.e. input variables, based on the concept of entropy (Nhu et al., 2020) that explains the most variance in the dataset. All new variables are orthogonal to each other, which in turn avoids the effect of multicollinearity and overfitting. From the statistical analysis presented above, it is evident that the degree of correlation between the attributes varies, whereby the mixed correlation leads to a multicollinearity effect in the model. Although the number of PCs generated through PCA is equal to the number of input variables, the optimal number of PCs can be selected based on the cumulative proportions of the variance. The descriptive details of PCs are presented in Table 4 including the standard deviation (SD), proportion of variance (POV) and cumulative proportion (CP) of all 13 PCs.

Further, the statistical details of each PC along with their loadings are given in Tables 5 and 6, respectively. The optimal number of PCs was selected (PC1–PC9) based on the Scree plot (Fig. 13a), which shows the percentage of explained variances by each PC. It is observed from the analysis that the first 9 PCs (PC1–PC9) contributed approximately 98% of total variance, while the contribution of the remaining PCs (PC10–PC13) was very nominal in terms of proportion of variance, which are likely unimportant. The graphical representation of PCs in terms of their SD, POV and CP is presented in Fig. 13b, in which the amount of contribution of the last 4 PCs can be visualized as well. There are no selection criteria for PCs, which mainly depend upon the choice of the individual researcher and the amount of cumulative variance needed to incorporate in the analysis.

As stated above, 5 ELM-based hybrid meta-heuristic models, namely ELM-HHO, ELM-IHHO, ELM-PSO, ELM-GA, and ELM-BBO, have been developed in this study. Before data processing, a dimension reduction technique i.e. PCA, was implemented to reduce the number of input variables through PCs. Based on the results of PCA, the first 9 PCs were selected considering the cumulative proportion of PCs, as the last 4 PCs contribute a very small fraction of the variability (about 1% and less) and are most likely insignificant.

4.4. Data processing and artificial intelligence-based analysis

Right after the selection of PCs, the entire dataset was normalized using the 'min-max' technique (Bardhan et al., 2021a). The most crucial stage in the field of soft computing is considered to be data normalization, which is a pre-processing activity in any problem. Generally, normalization of data is performed to nullify the dimensional effect of the variables. Thus, in the pre-processing phase, the 'min-max' normalization technique is used to normalize the data within a range defined by the upper limit of 1 and lower limit of 0. The main dataset was then partitioned into subsets for training and testing. For this, 75% (i.e. 516 samples) of the main dataset was randomly selected as the training subset, while the remaining 25% (i.e. 172 samples) was used as the testing subset. The 75:25 splitting ratio was chosen to implement 4-fold cross-validation and the development of a robust prediction model. The entire process presented in Fig. 14 shows the steps of the model, including dimension reduction of input parameters using PCA, selection of PCs, data normalization, data partitioning, and processing

Table 4
Realization of PCA.

Parameter	PC1	PC2	PC3	PC4	PC5	PC6	PC7	PC8	PC9	PC10	PC11	PC12	PC13
SD	2.02	1.63	1.29	1.18	0.87	0.8	0.76	0.69	0.64	0.42	0.37	0.03	0
POV	0.32	0.2	0.13	0.11	0.06	0.05	0.04	0.04	0.03	0.01	0.01	0	0
CP	0.32	0.52	0.65	0.76	0.81	0.86	0.91	0.94	0.98	0.99	1	1	1
Considered in analysis	Y	Y	Y	Y	Y	Y	Y	Y	Y	N	N	N	N

Note: Y = Yes, N = No.

Table 5
Statistical summary of PCs.

Parameter	PC1	PC2	PC3	PC4	PC5	PC6	PC7	PC8	PC9	PC10	PC11	PC12	PC13
Min	-5.61	-5.42	-3.84	-3.34	-3.07	-4.68	-1.86	-2.25	-2.95	-2.13	-1.14	-0.08	0.00
1st quartile	-1.3	-1.16	-0.88	-0.75	-0.46	-0.44	-0.47	-0.44	-0.38	-0.22	-0.22	-0.03	0.00
Median	-0.08	-0.01	-0.14	0.01	-0.06	0.02	-0.03	0.02	0.05	0.02	0.01	0.00	0.00
Mean	0	0	0	0	0	0	0	0	0	0	0	0.00	0.00
3rd quartile	1.35	1.03	0.81	0.75	0.36	0.45	0.49	0.42	0.41	0.28	0.22	0.03	0.00
Max	5.8	5.22	5.01	3.74	6.18	2.4	3.13	3.6	2.12	1.01	1.75	0.07	0.00
Standard error	0.08	0.06	0.05	0.05	0.03	0.03	0.03	0.03	0.02	0.02	0.01	0.00	0.00
SD	2.02	1.63	1.29	1.18	0.87	0.8	0.76	0.69	0.64	0.42	0.37	0.03	0.00
Variance	4.1	2.65	1.67	1.4	0.76	0.65	0.57	0.48	0.41	0.17	0.14	0.00	0.00
MAD	1.98	1.64	1.21	1.11	0.6	0.66	0.7	0.63	0.56	0.37	0.33	0.04	0.00
Trimmed	-0.01	-0.01	-0.05	0	-0.05	0.01	-0.01	-0.01	0.03	0.02	0	0.00	0.00
Skewness	0.04	0.07	0.4	-0.01	1.2	-0.49	0.25	0.27	-0.52	-0.86	0.05	-0.08	-0.31
Kurtosis	0	-0.02	0.21	0.22	5.96	2.62	0.63	1.53	1.63	2.71	0.92	-1.05	-0.08

Table 6
Details of loadings of PCs.

Parameter	PC1	PC2	PC3	PC4	PC5	PC6	PC7	PC8	PC9	PC10	PC11	PC12	PC13
D	0.3	0.31	0.38	–	0.12	–	0.23	–	–	0.49	0.6	–	–
Gs	0.36	−0.23	–	–	–	−0.24	–	−0.52	−0.56	0.33	−0.23	–	–
BD	0.35	0.36	–	0.32	–	–	−0.12	–	–	−0.18	−0.22	−0.74	–
DD	0.19	0.39	−0.17	0.37	−0.22	−0.15	−0.54	–	–	–	–	0.52	–
WC	0.38	0.15	0.3	0.1	0.18	–	0.46	–	–	−0.42	−0.35	0.43	–
G	–	0.29	−0.17	−0.49	−0.47	−0.22	0.26	−0.32	0.38	–	–	–	−0.2
CS	0.11	0.36	−0.26	−0.41	–	–	–	0.57	−0.54	–	–	–	−0.1
MS	–	0.25	−0.45	−0.1	0.76	–	–	−0.23	0.23	–	–	–	−0.18
FS	−0.38	0.11	0.35	0.12	0.13	−0.42	–	–	−0.18	−0.11	–	–	−0.68
MC	0.34	−0.33	−0.14	0.12	−0.19	0.47	–	0.12	0.12	–	–	–	−0.67
LL	0.37	−0.26	–	−0.22	0.18	−0.15	−0.35	−0.11	–	−0.55	0.51	–	–
PL	–	–	0.51	−0.49	–	–	−0.47	–	0.23	0.22	−0.38	–	–
FSI	0.25	−0.31	−0.17	–	0.11	−0.65	0.1	0.45	0.32	0.2	−0.1	–	–

and development of computational models, followed by a prediction of output at the end.

Ten widely used performance parameters were utilized to investigate the performance of the developed hybrid ELMs (Raja and Shukla, 2020, 2021a, b; Asteris et al., 2021a, b; Bardhan et al., 2021a, b, c; Ghani et al., 2021; Kaloop et al., 2021; Kardani et al., 2021a, b, c, d; Kumar et al., 2021; Raja et al., 2021), namely adjusted coefficient of determination ($Adj.R^2$), R^2, performance index (*PI*), variance account for (*VAF*), Willmott's index of agreement (*WI*), root mean square error (*RMSE*), mean absolute error (*MAE*), mean absolute percentage error (*MAPE*), mean bias error (*MBE*) and weighted mean absolute percentage error (*WMAPE*), which were determined and compared in every possible way. The mathematical equations of these indices are given below:

$$Adj.R^2 = 1 - \frac{n-1}{n-p-1}\left(1-R^2\right) \tag{31}$$

$$R^2 = \frac{\sum_{i=1}^{n}(y_i - y_{\text{mean}})^2 - \sum_{i=1}^{n}(y_i - \widehat{y}_i)^2}{\sum_{i=1}^{n}(y_i - y_{\text{mean}})^2} \tag{32}$$

$$PI = adj.R^2 + 0.01VAF - RMSE \tag{33}$$

$$VAF = \left[1 - \frac{\text{var}(y_i - \widehat{y}_i)}{\text{var}(y_i)}\right] \times 100\% \tag{34}$$

$$WI = 1 - \frac{\sum_{i=1}^{n}(y_i - \widehat{y}_i)^2}{\sum_{i=1}^{n}(|\widehat{y}_i - y_{\text{mean}}| + |y_i - y_{\text{mean}}|)^2} \tag{35}$$

$$RMSE = \sqrt{\frac{1}{n}\sum_{i=1}^{n}(y_i - \widehat{y}_i)^2} \tag{36}$$

$$MAE = \frac{1}{n}\sum_{i=1}^{n}|(\widehat{y}_i - y_i)| \tag{37}$$

$$MAPE = \frac{1}{n}\sum_{i=1}^{n}\left|\frac{y_i - \widehat{y}_i}{y_i}\right| \times 100\% \tag{38}$$

$$MBE = \frac{1}{n}\sum_{i=1}^{n}(\widehat{y}_i - y_i) \tag{39}$$

$$WMAPE = \frac{\sum_{i=1}^{n}\left|\frac{y_i - \widehat{y}_i}{y_i}\right| y_i}{\sum_{i=1}^{n} y_i} \tag{40}$$

where n indicates the number of observations of the respective parameter; p represents the number of input parameters considered in developing the predictive model; y_i and $\widehat{y}_i$ are the actual and modeled ith values of the desired output, i.e. C_c; and y_{mean} is the average of the input variables. The values of these indices should be identical to their ideal values for a perfect prediction model (Table 7).

In addition to the above performance indices, a new index called performance strength (*PS*) is introduced in this study which is an integration of four performance parameters, namely $adj.R^2$,

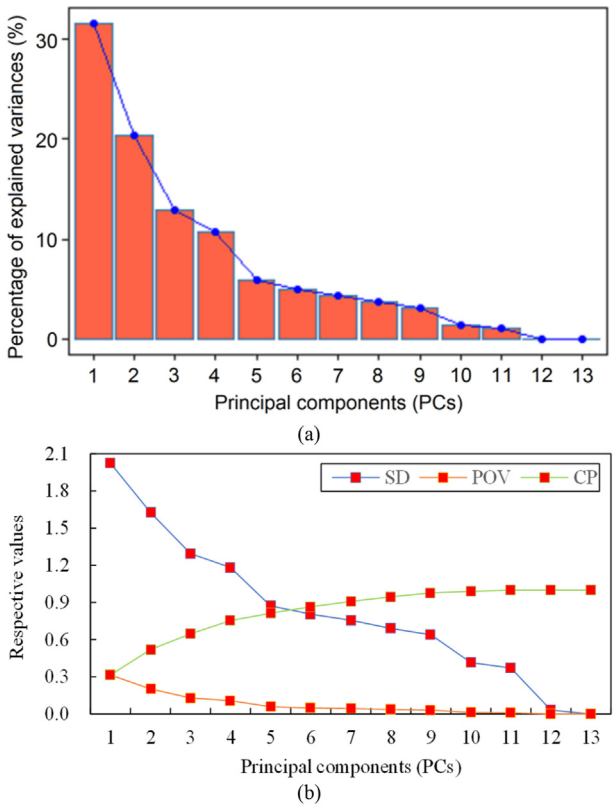

Fig. 13. (a) Scree plot of PCs showing the percentage of explained variances; and (b) Plot of PCs vs. SD, POV, and CP.

R^2, *VAF* and *RMSE*. The idea behind the implementation of this index is to evaluate the relative efficiency of the predictive model considering the values of $Adj.R^2$, *VAF* and *RMSE* for the total dataset to the values of $Adj.R^2$ and R^2 in the training and testing subsets. In general, $Adj.R^2$ aids in determining how much the predictive association with the index is due to the inclusion of those factors, i.e. it compensates for the addition of variables and only increases if the new predictor enhances the model when it is above the value obtained by probability. Conversely, it will decrease if a predictor improves the model when it is less than that predicted by chance. Therefore, $Adj.R^2$ plays an important statistical role in artificial intelligence-based analysis and should

Table 7
Ideal values of different statistical parameters.

$Adj.R^2$	R^2	*PI*	*VAF* (%)	*WI*	*RMSE*	*MAE*	*MAPE*(%)	*MBE*	*WMAPE*
1	1	2	100	1	0	0	0	0	0

be considered by researchers for comparative assessment of the training and testing outcomes. In this work, the new *PS* index can be defined as follows:

$$PS = \frac{\left(Adj.R^2\right)_{\text{total}} + (0.01VAF)_{\text{total}} - (RMSE)_{\text{total}}}{\left(\frac{Adj.R^2}{R^2}\right)_{\text{training}} + \left(\frac{Adj.R^2}{R^2}\right)_{\text{testing}}} \tag{41}$$

Importantly, *PS* can estimate the strength of performance of a predictive model by comparing the values of $Adj.R^2$ and R^2 for both training and testing datasets along with the values of *VAF* and *RMSE* for the total dataset. The ideal value of *PS* is 1.

5. Results and discussion

This section presents the results of the proposed hybrid ELMs in predicting C_c of soils. For this purpose, 13 soil parameters (i.e. *D*, *Gs*, *BD*, *DD*, *WC*, *G*, *CS*, *MS*, *FS*, *MC*, *LL*, *PL* and *FSI*) were analyzed. Before training the models, the dimension reduction technique was implemented to reduce the number of input features as well as the multicollinearity effect between the parameters. The number of input variables was then selected through PCs based on cumulative proportions of variance. Subsequently, the training dataset (516 observations) and testing dataset (172 observations) were employed to develop and validate the models, respectively. The outcomes of all developed models are furnished in the following sub-sections. Ultimately, the best predictive model was determined through the proposed statistical parameter called *PS*.

Before reviewing the results of the developed ELMs, the parametric configurations along with their optimum values are presented in Table 8. As mentioned earlier, to construct the optimum hybrid model, it is necessary to tune the deterministic parameter of MOAs along with the number of hidden neurons (n_h) of ELM. In this work, n_h ranging from 5 to 25 has been examined to obtain the optimized weights and biases of the connecting neurons. After a preliminary trial-and-error run, the optimum values of n_h was determined to be 15. Also, other deterministic parameters, such as particle/swarm/population size (n_p), maximum number of iterations (t), C_1 and C_2, w_{max} and w_{min}, upper and lower bounds (*UB*

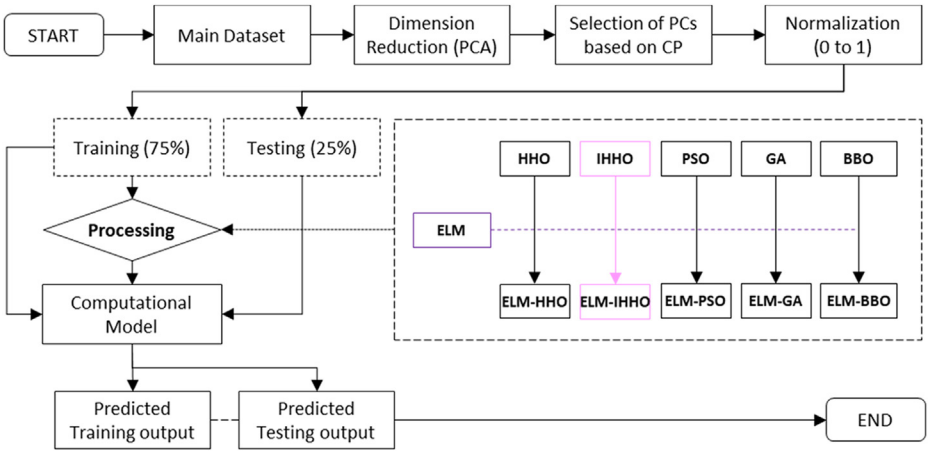

Fig. 14. Flowchart showing steps in the application of artificial intelligence models.

and *LB*), and other parameters of MOAs, were tuned during simulations. The most effective choices of these parameters obtained in each case with their optimal value are provided in Table 8. When the training of hybrid ELMs was completed, the final structure of each model was finalized. The number of learning parameters optimized in ELM-based modeling is equal to 150 (i.e. $15 \times 9 + 15$). To compare the suggested models fairly, the optimum n_h achieved in the ELM-HHO model was applied for the other models and kept constant throughout the investigation. Note that, to choose the most significant testing datasets, 4-fold cross-validation was used. Thus, the main dataset was partitioned into 4 equal parts. Among them, a single subset was chosen as the testing dataset, while the others were used as the training dataset. The goal of using cross-validation was to build the model more efficiently so that the highest prediction accuracy could be reached during the validation phase. The most effective testing dataset discovered through ELM-HHO modeling was utilized to model other hybrid models including ELM-HHO, ELM-IHHO, ELM-PSO, ELM-GA, and ELM-BBO, the detailed procedures of which are discussed below.

The ELM was initially initialized in ELM-HHO modeling, and then the HHO algorithm was incorporated to optimize the weights and biases of ELM for predicting C_c of soils. During the optimization, the *RMSE* and sigmoid function were used as the fitness function and activation function, respectively, in each iteration. The searching operation was performed in 5000 iterations with $n_p = 10–25$, to ensure the most efficient search for the weights and biases, as well as other parameters of the chosen ELM-HHO model. To achieve stable convergence, the value of t was set to 5000. Ultimately, the optimum value of deterministic parameter of ELM obtained from trial-and-error run is $n_h = 15$. $n_p = 25$ was obtained as the optimum. The optimized values of weights and biases of connecting neurons were then used to predict a new set of data, i.e. testing dataset. The performance of 4-fold cross-validation (based on R^2 value) is also presented in Fig. 15. In addition, the predictive performances of both training and testing subsets of the ELM-HHO model are illustrated in Figs. 16a and 17a, respectively.

Similar to the ELM-HHO model, after the initialization of ELM, the mutation-based IHHO was used to optimize ELM's learning parameters. Using the same optimum values of HHO parameters, the ELM-IHHO model was trained. The mutation parameters of IHHO algorithm were set to: mutation = 0.05%, mutation probability = 0.001, $n_h = 15$, $n_p = 25$, and $t = 5000$. Subsequently, the optimized values of weights and biases of the connecting neurons were used for predicting a new dataset, i.e. the testing dataset. The predictive results of C_c prediction in the training and testing phases are illustrated in Figs. 16b and 17b, respectively. Note that, although the values of n_h, n_p, and t are the same, the optimum values of weights and biases of the ELM-IHHO model are different.

The steps applied for ELM-HHO and ELM-IHHO modeling were followed to optimize the weights and biases of ELM using PSO, GA, and BBO. For this, the parameters of PSO, GA, and BBO were tuned by the trial-and-error method to obtain the best predictive model of ELM-PSO, ELM-GA, and ELM-BBO in each case. The values of n_h, n_p, and t were kept constant for all cases. In PSO, the optimum values of parameters were determined as: $C_1 = 1$, $C_2 = 2$, $w_{max} = 0.9$, and $w_{min} = 0.4$. In GA, the optimal parameters were: mutation probability = 0.001, gamma = 0.8 and sigma = 0.5. In BBO, the required parameters before optimizing the ELM were: kept habitats (Elitism) = 0.5, immigration (I) = 1, emigration (E) = 1, and mutation probability = 0.001. Finally, the optimized ELM-PSO, ELM-GA, and ELM-BBO models with optimal values of weights and biases were chosen based on the lowest *RMSE*. The predictive results for the training and testing datasets are shown in Fig. 16c–e and 17c–e, respectively. In addition, the error histogram (for the whole dataset) of the developed models is shown in Fig. 18.

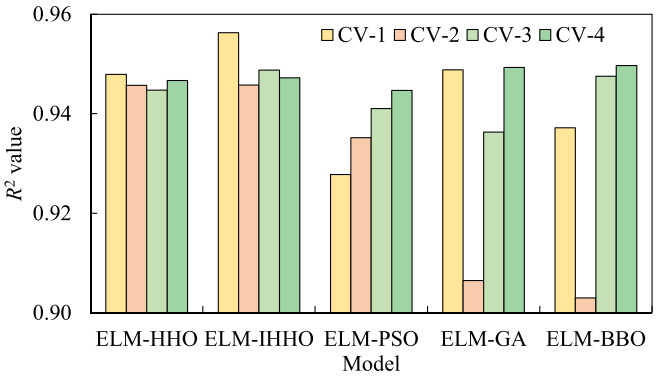

Fig. 15. Bar plot of 4-fold cross-validation (CV-1 to CV-4) results (based on R^2 values).

Furthermore, the convergence curve of MOAs is very important in assessing their performance, which indicates the ability of the optimization algorithm to escape from local optima. Local optima are more likely to occur in algorithms with an unbalanced exploration and exploitation issue. A comparison between ELM-IHHO convergence and the other algorithms, i.e. ELM-HHO, ELM-PSO, ELM-GA, and ELM-BBO, is shown in Fig. 19. The convergence curves show that IHHO achieved a better solution faster than ELM-based MOAs, proving the IHHO algorithm's superiority in ELM-IHHO modeling. The effectiveness of the proposed ELM-IHHO model can be assessed based on the bar plot shown inside Fig. 19, in which the computational time of all the algorithms is presented in graphical form. After completion of 5000 iterations, the computational time was calculated as 365.22 s for HHO, 138.98 s for IHHO, 316.88 s for PSO, 649.87 s for GA, and 570.33 s for BBO. Furthermore, considering that the proposed IHHO algorithm consumed 61.94% less computational time compared to the HHO algorithm, it offers a more efficient and robust algorithm.

In the following sub-sections, the realizations of the developed models in predicting C_c are assessed in detail. The predictive assessment based on performance indices is presented and discussed first. This is followed by visual interpretation and accuracy analysis of the results, including the Taylor diagram, accuracy matrix and analysis of the newly proposed index, *PS*. In the end, a discussion on the generalization capability of the proposed models is presented.

5.1. Statistical details of results

After the development of the models, their efficiency and generalization capability were assessed through several performance indices, as listed above. Specifically, the values of 10

Table 8
Details of different parameters of the MOAs.

Optimization parameters	HHO	IHHO	PSO	GA	BBO
n_h	15	15	15	15	15
t	5000	5000	5000	5000	5000
n_p	25	25	25	25	25
UB, *LB*	±1	±1	±1	±1	±1
C_1, C_2	–	–	1, 2	–	–
w_{max}, w_{min}	–	–	0.9, 0.4	–	–
Gamma	–	–	–	0.8	–
Sigma	–	0.5	–	0.5	–
Kept habitats (Elitism)	–	–	–	–	0.5
Immigration (I), Emigration (E)	–	–	–	–	1, 1
Mutation (%)	–	0.5	–	–	–
Mutation probability	–	0.001	–	0.001	0.001

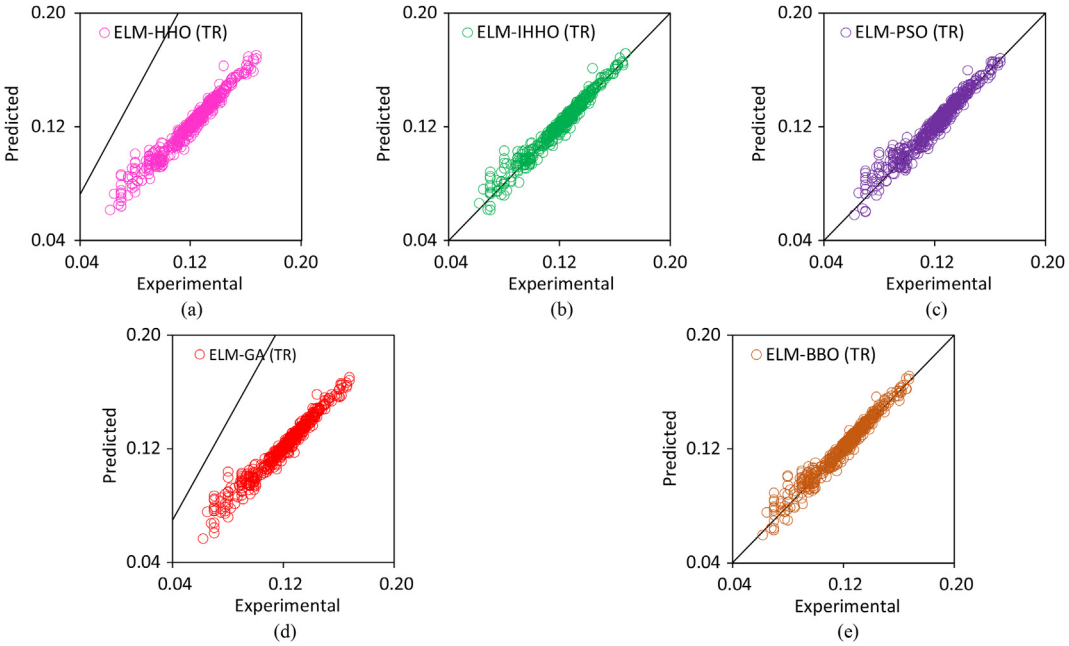

Fig. 16. Illustration of experimental vs. estimated values of the proposed ELMs in the training (TR) phase.

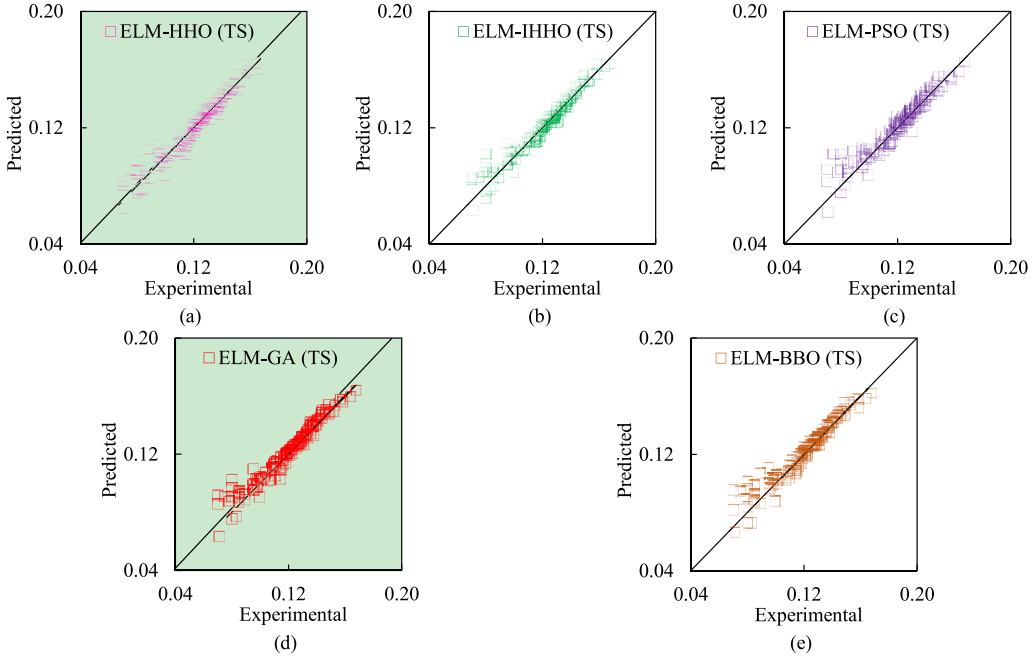

Fig. 17. Illustration of experimental vs. estimated values of the proposed ELMs in the testing (TS) phase.

performance indices (*Adj*.R^2, R^2,*PI*, *VAF*, *WI*, *RMSE*, *MAE*, *MAPE*, *MBE*, and *WMAPE*) for all the five models were determined separately for the training and testing datasets, as shown in Tables 9 and 10, respectively. The results show that all of the models capture the relationship between soil parameters and consolidation parameters in estimating soil C_c. As can be seen, the proposed models achieved more than 95% accuracy in the training stage based on R^2 values, which indicates that the models fit well with the experimental results. These outcomes demonstrate that the proposed ELM-based meta-heuristic models exhibit good predictive performance. Also, the values of other indices, i.e. *Adj*.R^2 *PI*, *MAPE*, *MBE* and *WMAPE*, indicate good predictive accuracy. However, a comprehensive review of the results reveals that the ELM-IHHO and ELM-HHO models, achieved almost equal predictive performance in the training stage, while the performances of ELM-PSO and ELM-BBO were reduced significantly in the testing phase.

5.2. Visual interpretation of results and accuracy analysis

5.2.1. Taylor diagram

The Taylor diagram, invented by Taylor (2001), is a 2D mathematical diagram designed to graphically indicate which of several models is most realistic. In other words, this diagram provides a comparative and graphical assessment of different models in a

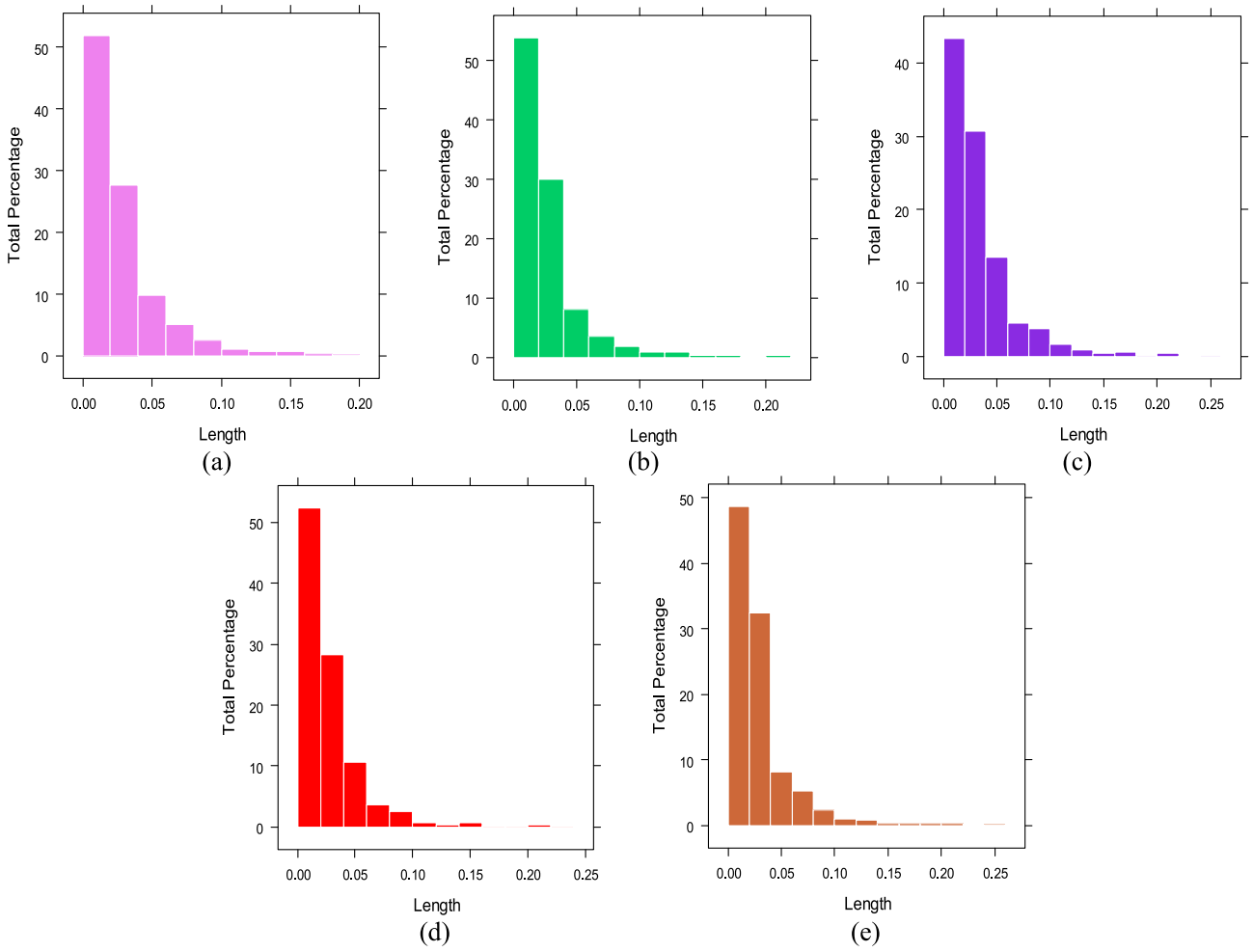

Fig. 18. Illustration of error histogram (for all datasets): (a) ELM-HHO, (b) ELM-IHHO, (c) ELM-PSO, (d) ELM-GA, and (e) ELM-BBO.

single figure. The degree of correspondence between the actual and predicted behaviors is quantified in terms of their values of *R*, *RMSE*, and the ratio of SD, and indicated by a single point. For an ideal model, the position of the point should be closer to the reference point (Ref). Relative merits of the models proposed in this study can be inferred from Fig. 20, in which the status of the models is shown by points (different markers). As can be seen, the ELM-IHHO model appears closer to the reference point (Ref) and, therefore, can be considered as the most robust model.

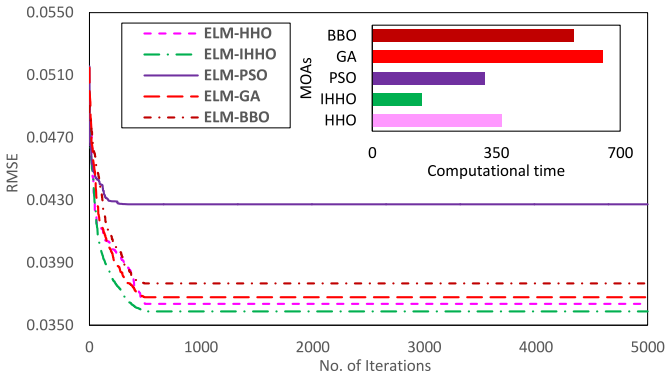

Fig. 19. Convergence curve and computational time of the proposed ELMs.

5.2.2. Accuracy matrix

This sub-section presents a novel graphical representation of the proposed hybrid models in the form of a heat-map matrix called the accuracy matrix, in which the values of performance parameters are presented in terms of accuracies (in %) achieved based on their ideal values. In other words, the amount of accuracy of the proposed models is calculated against the ideal values of each performance index and presented accordingly. The expressions given in Eqs. (42) and (43) were used to calculate the amount of accuracy in the percentage of the predictive model. For the trend measuring parameters (*Adj*.R^2, R^2, *PI*, *VAF* and *WI*), Eq. (42) was used, while Eq. (43) was employed for the error measuring parameters (*RMSE*, *MAE*, *MBE*, *MAPE* and *WMAPE*), respectively:

$$A_t = \frac{|p_a|}{i_a} \times 100\% \tag{42}$$

$$A_e = |1 - |p_e|| \times 100\% \tag{43}$$

where A_t and A_e indicate the error terms; i_a is the ideal value of trend measuring parameters; and p_a and p_e are the values of trend and error measuring parameters of the developed models, respectively. The error parameter indicating the percentage of error (such as *MAPE*) should be processed on the decimal scale.

One can easily visualize the minimum and maximum values of accuracy attained in each model. The overall accuracy of the proposed models can also be interpreted from the heat-map matrix. As

Table 9
Performance of the developed ELMs (training phase).

Model	*Adj.* R^2	R^2	*PI*	*VAF* (%)	*WI*	*RMSE*	*MAE*	*MAPE* (%)	*MBE*	*WMAPE*
ELM-HHO	0.9664	0.9672	1.8972	96.7194	0.991	0.0364	0.0258	8.418	0.01	0.0466
ELM-IHHO	0.9674	0.9682	1.8997	96.8212	0.9912	0.0359	0.0247	8.7296	0.0101	0.0444
ELM-PSO	0.9531	0.9543	1.8647	95.4283	0.9874	0.0427	0.0307	10.4894	0.011	0.0554
ELM-GA	0.966	0.9669	1.8961	96.6868	0.9907	0.0368	0.026	8.9673	0.0109	0.0468
ELM-BBO	0.964	0.965	1.8913	96.4949	0.9903	0.0377	0.0267	9.2898	0.0106	0.0482

Table 10
Performance of the developed ELMs (testing phase).

Model	*Adj.* R^2	R^2	*PI*	*VAF* (%)	*WI*	*RMSE*	*MAE*	*MAPE* (%)	*MBE*	*WMAPE*
ELM-HHO	0.9436	0.9479	1.8461	94.785	0.9853	0.0453	0.0319	10.8494	0.0122	0.0574
ELM-IHHO	0.9527	0.9563	1.8671	95.6279	0.9876	0.0419	0.0286	10.254	0.0126	0.0516
ELM-PSO	0.9218	0.9277	1.796	92.6923	0.9794	0.0527	0.0356	12.7905	0.0104	0.0641
ELM-GA	0.9446	0.9488	1.8477	94.8451	0.9851	0.0454	0.0298	11.0997	0.0132	0.0537
ELM-BBO	0.932	0.9372	1.819	93.6737	0.9819	0.0498	0.0325	12.0347	0.0128	0.0586

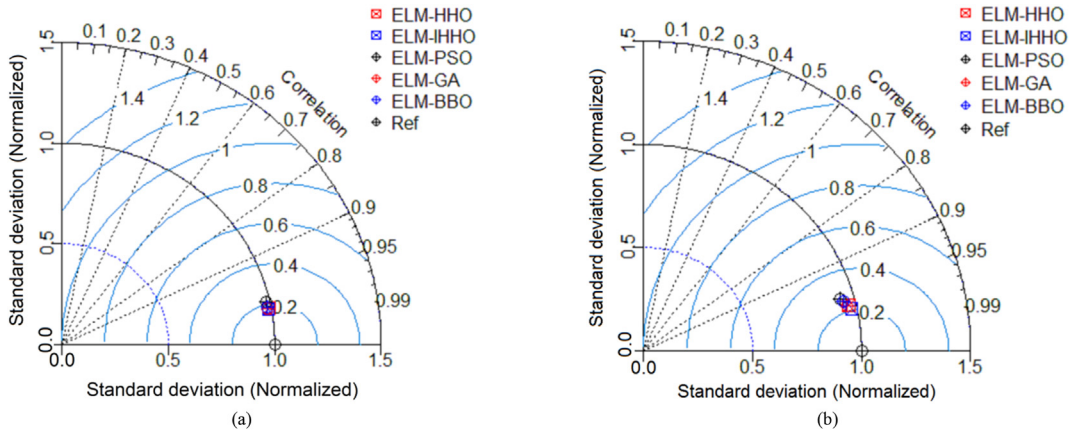

Fig. 20. Taylor diagrams for the (a) training and (b) testing phases.

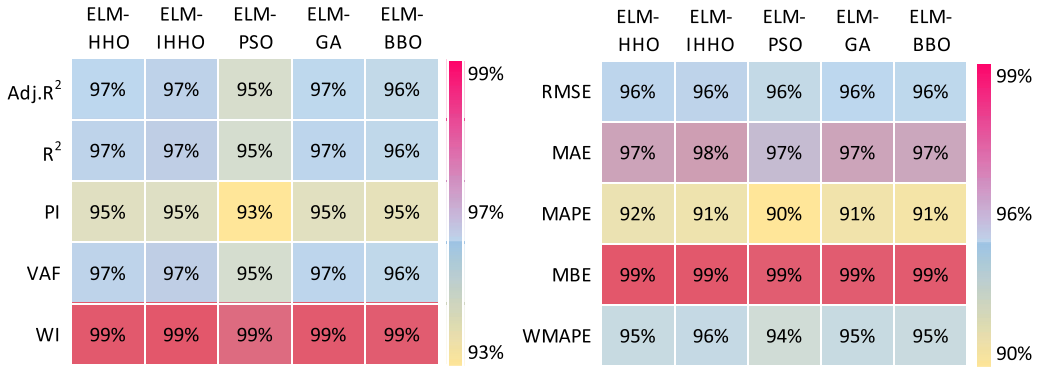

Fig. 21. Accuracy matrix for training results.

can be seen for Figs. 21 and 22, the minimum value of accuracy attained was 90% in terms of trend measuring parameters and 87% in terms of error measuring parameters, while maximum accuracy of 99% was observed in terms of both trend and error measuring parameters. Furthermore, the heat-map matrix is useful for quick assessment of any predictive model, which provides both minimum and maximum values of accuracy attained in each model and also pertinent information concerning the amount of error involved.

5.2.3. Analysis of performance strength

Furthermore, the proposed performance index, i.e. *PS*, was analyzed at the end of the study. This index was established since, generally, the performance indices determined separately for the training and testing datasets do not provide the overall accuracy of the models. As stated earlier, this index is highly effective in determining the overall accuracy and robustness of any predictive model. Using the expression in Eq. (41), the values of *PS* of all developed

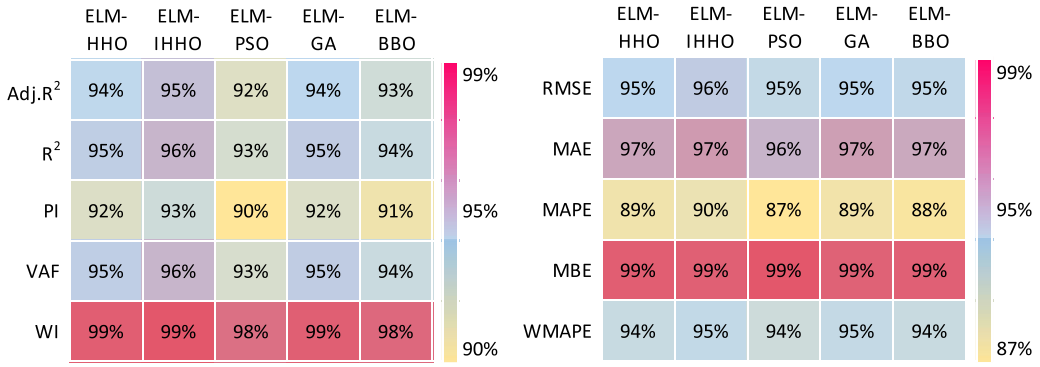

Fig. 22. Accuracy matrix for testing results.

models were calculated and are provided in Table 11. Also, the *PS* values are graphically represented in a bar plot in Fig. 23, which reveals that the ELM-IHHO model outperforms other hybrid ELMs. In addition, $PS = 0.9484$ was achieved by the ELM-IHHO model. Also, the ELM-HHO model was found to be the 2nd best model in terms of *PS* value, followed by ELM-GA, ELM-BBO and ELM-PSO.

5.3. Discussion of results

This sub-section builds upon the discussion of the outcomes of the proposed ELMs in the previous sub-section. According to the experimental results, all the proposed hybrid ELMs capture the relationship between soil characteristics and consolidation parameter in determining soil C_c. The suggested hybrid models showed a strong fit with the experimental dataset, with $R^2 > 0.9$ in both training and testing phases. Distinctively, the ELM-IHHO model achieved superior performance with $R^2 = 0.9682$, $RMSE = 0.0359$ and $MAE = 0.0247$ in the training stage, and $R^2 = 0.9563$, $RMSE = 0.0419$, and $MAE = 0.0286$ in the testing phase. Compared to the ELM-IHHO model, the ELM-GA model achieved almost an equal degree of fitting in the testing phase. However, the illustration of actual and predicted values exhibits that the predicted values are more scattered below the mean of soil C_c than those above mean value. This is mainly due to the presence of a wide range of experimental data of ML, ML-CL, and SM-SC soils with lower C_c values.

Nonetheless, to better demonstrate the capability of the proposed models, graphical interpretations of convergence curve, Taylor diagram, and accuracy matrix are described. Moreover, the robustness of the best predictive model was assessed through *PS*, a novel performance parameter proposed in this study. According to the findings, the ELM-IHHO model had the best predictive performance with $PS = 0.9484$, followed by the ELM-HHO, ELM-HHO, ELM-BBO, and ELM-PSO. Therefore, the ELM-IHHO model is indeed helpful in predicting the C_c value of soils and can be considered a robust model.

6. Summary and conclusions

It is well understood that reliable and accurate estimation of the soil compression index can save the time and cost of analysis needed before laying the foundation of a structure as well. The present study introduces 5 meta-heuristic hybrid models that combine MOAs, namely HHO, PSO, GA, BBO and ELM, and the novel mutation-based ELM-IHHO, to estimate soil C_c. For this purpose, 688 oedometer test data belonging to 6 different groups were obtained from a DFC project in India. ELM was employed to construct the mapping function that infers the value of C_c from a set of input parameters, while the other MOAs were used to optimize the weights and biases of the connecting neurons of ELM. In contrast, to ameliorate the efficiency of the data analysis process, the dimension reduction technique, i.e. PCA, was employed before training the models. The input parameters were then selected based on cumulative proportions of variance of PCs. In the next stage, the main dataset was divided into training and testing subsets, which were used to train and validate the developed models, respectively. Following the development of the models, several performance indices were determined to assess their predictive accuracy and generalization capability. Experimental results show that ELM-IHHO achieved the most desired accuracy in both phases. In the testing phase, no substantial variations or undesirable values were found, indicating that the models' generalization capabilities and robustness are satisfactory. In addition, the values of R^2 were greater than 0.9 in both phases, indicating that the proposed models fit well with the experimental dataset. The ELM-IHHO model can be deemed a promising technique for predicting soil C_c based on the results.

The goal of this study was to minimize the need for actual laboratory testing and to provide adequate details of prior artificial intelligence-based investigations, including their results at all levels. In order to address the gaps and limitations of earlier studies, the ELM-based HHO method (ELM-HHO) was built using a recently developed MOA, named HHO. Subsequently, an improvement of the standard HHO algorithm called IHHO was conducted using the

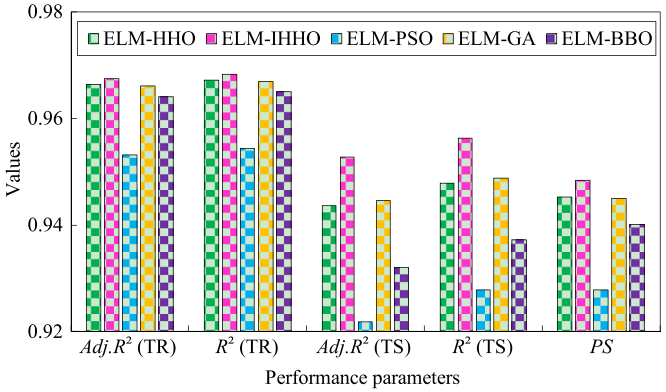

Fig. 23. Bar plot of *PS* values of the proposed models.

Table 11
Values of *PS* and rank of the developed models.

Model	*PS* value	Rank
ELM-HHO	0.9452	2
ELM-IHHO	0.9484	1
ELM-PSO	0.9279	5
ELM-GA	0.9449	3
ELM-BBO	0.9401	4

mutation-based search mechanism to expand the global and local searches of standard HHO. The experimental outcomes exhibit that the proposed ELM-IHHO model yields the most desired predictive performance in terms of computational time, convergence speed, and performance indices. The results also show that the ELM-IHHO model outperforms the other studied models. The main advantages of the proposed ELM-IHHO model include: higher predictive accuracy, optimized learning parameters, robustness, and accelerated convergence rate. Considering these advantages, the suggested ELM-IHHO model can be regarded as a potential method for dealing with real-world engineering problems, including soil C_c.

The future direction of this study may include: implementation of different dimension reduction techniques (such as kernel PCA, independent component analysis) for handling multicollinearity related issues in solving real-world problems of various engineering disciplines, improvement of other meta-heuristic algorithms using the concept (a mutation-based mechanism) proposed in this study, and further assessment of ELM-IHHO model using real-world data from different fields. However, as per the authors' knowledge, this study presents the first-time application of an ELM-based hybrid meta-heuristic optimization model for predicting C_c of soils.

Declaration of competing interest

The authors declare that they have no known competing financial interests or personal relationships that could have appeared to influence the work reported in this paper.

Acknowledgments

The authors are very thankful to the Dedicated Freight Corridor of India Limited (DFCCIL), New Delhi, India and officials of L&T Construction, DFCCIL CTP-3(R) Project Site, Ahmedabad, India to provide experimental data and their kind support during this study.

Appendix A. Supplementary data

Supplementary data to this article can be found online at https://doi.org/10.1016/j.jrmge.2021.12.018.

References

Acharyya, R., Dey, A., 2019. Assessment of bearing capacity for strip footing located near sloping surface considering ANN model. Neural Comput. Appl. 31, 8087–8100.

Alam, S., Khuntia, S., Patra, C., 2014. Prediction of compression index of clay using artificial neural network. In: International Conference on Industrial Engineering Science and Applications. National Institute of Technology, Durgapu, West Bengal, India.

Alizadeh Majdi, A., Dabiri, R., Ganjian, N., Ghalandarzadeh, A., 2019. Determination of the soil compression index (C_c) in clayey soils using shear wave velocity (Case study: Tabriz City). Iran. J. Sci. Technol. Trans. Civ. Eng. 43, 577–588.

Armaghani, D.J., Asteris, P.G., 2020. A comparative study of ANN and ANFIS models for the prediction of cement-based mortar materials compressive strength, Neural Comput. Appl 33, 4501–4532.

Armaghani, D.J., Hajihassani, M., Mohamad, E.T., Marto, A., Noorani, S.A., 2014. Blasting-induced flyrock and ground vibration prediction through an expert artificial neural network based on particle swarm optimization. Arabian J. Geosci. 7, 5383–5396.

Asmawisham Alel, M.N., Anak Upom, M.R., Abdullah, R.A., Zainal Abidin, M.H., 2018. Optimizing blasting's air overpressure prediction model using swarm intelligence. J. Phys. Conf. Ser. 995, 012046.

Asteris, P.G., Skentou, A.D., Bardhan, A., Samui, P., Lourenço, P.B., 2021a. Soft computing techniques for the prediction of concrete compressive strength using non-destructive tests. Construct. Build. Mater. 303, 124450.

Asteris, P.G., Skentou, A.D., Bardhan, A., Samui, P., Pilakoutas, K., 2021b. Predicting concrete compressive strength using hybrid ensembling of surrogate machine learning models. Cement Concr. Res. 145, 106449.

Bardhan, A., Gokceoglu, C., Burman, A., Samui, P., Asteris, P.G., 2021b. Efficient computational techniques for predicting the California bearing ratio of soil in soaked conditions. Eng. Geol. 291, 106239.

Bardhan, A., Manna, P., Kumar, V., Burman, A., Žlender, B., Samui, P., 2021c. Reliability analysis of piled raft foundation using a novel hybrid approach of ANN and equilibrium optimizer. Comput. Model. Eng. Sci. 128 (3), 1033–1067.

Bardhan, A., Samui, P., Ghosh, K., Gandomi, A.H., Bhattacharyya, S., 2021a. ELM-based adaptive neuro swarm intelligence techniques for predicting the California bearing ratio of soils in soaked conditions. Appl. Soft Comput. 110, 107595.

Benbouras, M.A., Mitiche, R.K., Zedira, H., Petrisor, A.I., Mezouar, N., Debiche, F., 2019. A new approach to predict the compression index using artificial intelligence methods. Mar. Georesour. Geotechnol. 37 (6), 704–720.

Bui, D.T., Nhu, V.H., Hoang, N.D., 2018. Prediction of soil compression coefficient for urban housing project using novel integration machine learning approach of swarm intelligence and multi-layer perceptron neural network. Adv. Eng. Inf. 38, 593–604.

Cai, R., Han, T., Liao, W., Huang, J., Li, D., Kumar, A., Ma, H., 2020. Prediction of surface chloride concentration of marine concrete using ensemble machine learning. Cement Concr. Res. 136, 106164.

Chen, L., Zhang, W., Gao, X., Wang, L., Li, Z., Böhlke, T., Perego, U., 2020. Design Charts for Reliability Assessment of Rock Bedding Slopes Stability against Biplanar Sliding: SRLEM and BPNN Approaches. Georisk. https://doi.org/10.1080/17499518.2020.1815215.

Cozzolino, V.M., 1961. Statistical forecasting of compression index. In: Proceedings of the 5th International Conference on Soil Mechanics and Foundation Engineering, Paris, France, pp. 51–53.

Farswan, P., Bansal, J.C., Deep, K., 2016. A modified biogeography based optimization. In: Kim, J., Geem, Z. (Eds.), Harmony Search Algorithm, Advances in Intelligent Systems and Computing, vol. 382. Springer, Berlin, Heidelberg, pp. 227–238.

Gandomi, A.H., Yang, X.S., Talatahari, S., Alavi, A.H., 2013. Metaheuristic algorithms in modeling and optimization. In: Gandomi, A.H., Yang, X.S., Talatahari, S., Alavi, A.H. (Eds.), Metaheuristic Applications in Structures and Infrastructures. Elsevier, London, UK, pp. 1–24.

Ghani, S., Kumari, S., Bardhan, A., 2021. A novel liquefaction study for fine-grained soil using PCA-based hybrid soft computing models. Sādhanā 46, 113.

Goh, A.T.C., Zhang, R.H., Wang, W., Wang, L., Liu, H.L., Zhang, W.G., 2020. Numerical study of the effects of groundwater drawdown on ground settlement for excavation in residual soils. Acta Geotech 15, 1259–1272.

Goh, A.T.C., Zhang, W., Zhang, Y., Xiao, Y., Xiang, Y., 2018. Determination of earth pressure balance tunnel-related maximum surface settlement: a multivariate adaptive regression splines approach. Bull. Eng. Geol. Environ. 77, 489–500.

Goh, A.T.C., Zhang, Y., Zhang, R., Zhang, W., Xiao, Y., 2017. Evaluating stability of underground entry-type excavations using multivariate adaptive regression splines and logistic regression. Tunn. Undergr. Space Technol. 70, 148–154.

Golafshani, E.M., Behnood, A., Arashpour, M., 2020. Predicting the compressive strength of normal and high-performance concretes using ANN and ANFIS hybridized with grey wolf optimizer. Construct. Build. Mater. 232, 117266.

Hajihassani, M., Armaghani, D.J., Sohaei, H., Mohamad, E.T., Marto, A., 2014. Prediction of airblast-overpressure induced by blasting using a hybrid artificial neural network and particle swarm optimization. Appl. Acoust. 80, 57–67.

Hasanipanah, M., Armaghani, D.J., Amnieh, H.B., Majid, M.Z.A., Tahir, M.M.D., 2017. Application of PSO to develop a powerful equation for prediction of flyrock due to blasting. Neural Comput. Appl. 28, 1043–1050.

Heidari, A.A., Mirjalili, S., Faris, H., Aljarah, I., Mafarja, M., Chen, H., 2019. Harris hawks optimization: algorithm and applications. Future Generat. Comput. Syst. 97, 849–872.

Holland, J.H., 1992. Genetic algorithms. Sci. Am. 267, 66–72.

Huang, G.B., Zhu, Q.Y., Siew, C.K., 2006. Extreme learning machine: theory and applications. Neurocomputing 70, 489–501.

Jia, H., Lang, C., Oliva, D., Song, W., Peng, X., 2019. Dynamic harris hawks optimization with mutation mechanism for satellite image segmentation. Rem. Sens. 11, 1421.

Jia, H.Z., Nee, A.Y.C., Fuh, J.Y.H., Zhang, Y.F., 2003. A modified genetic algorithm for distributed scheduling problems. J. Intell. Manuf. 14, 351–362.

Kaloop, M.R., Bardhan, A., Kardani, N., Samui, P., Hu, J.W., Ramzy, A., 2021. Novel application of adaptive swarm intelligence techniques coupled with adaptive network-based fuzzy inference system in predicting photovoltaic power. Renew. Sustain. Energy Rev. 148, 111315.

Kardani, N., Bardhan, A., Gupta, S., Samui, P., Nazem, M., Zhang, Y., Zhou, A., 2021a. Predicting permeability of tight carbonates using a hybrid machine learning approach of modified equilibrium optimizer and extreme learning machine. Acta Geotech. https://doi.org/10.1007/s11440-021-01257-y.

Kardani, N., Bardhan, A., Kim, D., Samui, P., Zhou, A., 2021b. Modelling the energy performance of residential buildings using advanced computational frameworks based on RVM, GMDH, ANFIS-BBO and ANFIS-IPSO. J. Build. Eng. 35, 102105.

Kardani, N., Bardhan, A., Roy, B., Samui, P., Nazem, M., Armaghani, D.J., Zhou, A., 2021c. A novel improved Harris Hawks optimization algorithm coupled with ELM for predicting permeability of tight carbonates. Eng. Comput. https://doi.org/10.1007/s00366-021-01466-9.

Kardani, N., Bardhan, A., Samui, P., Nazem, M., Zhou, A., Armaghani, D.J., 2021d. A novel technique based on the improved firefly algorithm coupled with

extreme learning machine (ELM-IFF) for predicting the thermal conductivity of soil. Eng. Comput.
Kashefipour, S.M., Daryaee, M., 2014. Modeling the compression index for fine soils using an intelligent method. J. Biodivers. Environ. Sci. (JBES) 5, 197–204.
Kennedy, J., Eberhart, R., 1995. Particle swarm optimization. In: Proceedings of International Conference on Neural Networks (ICNN'95). IEEE, New York, USA, pp. 1942–1948.
Kolay, P.K., Rosmina, A.B., Shirley, Y., 2011. Prediction of compression index for tropical soil by using artifi cial neural network (ANN). Comput. Methods Geomech. Front. New Appl. 1, 542–547.
Koopialipoor, M., Fallah, A., Armaghani, D.J., Azizi, A., Mohamad, E.T., 2019. Three hybrid intelligent models in estimating flyrock distance resulting from blasting. Eng. Comput. 35, 243–256.
Kordnaeij, A., Kalantary, F., Kordtabar, B., Mola-Abasi, H., 2015. Prediction of recompression index using GMDH-type neural network based on geotechnical soil properties. Soils Found. 55 (6), 1335–1345.
Kumar, M., Bardhan, A., Samui, P., Hu, J.W., Kaloop, M.R., 2021. Reliability analysis of pile foundation using soft computing techniques: a comparative study. Processes 9 (3), 486.
Kurnaz, T.F., Dagdeviren, U., Yildiz, M., 2016. Prediction of Compressibility Parameters of the Soils Using Artificial Neural Network, 1, vol. 5. Springerplus, p. 1801. Ozkan, O.
Kurnaz, T.F., Kaya, Y., 2018. The comparison of the performance of ELM, BRNN, and SVM methods for the prediction of compression index of clays. Arabian J. Geosci. 11, 770.
Le, L.T., Nguyen, H., Dou, J., Zhou, J., 2019. A comparative study of PSO-ANN, GA-ANN, ICA-ANN, and ABC-ANN in estimating the heating load of buildings' energy efficiency for smart city planning. Appl. Sci. 9 (13), 2630.
Li, C., 2014. A simplified method for prediction of embankment settlement in clays. J. Rock Mech. Geotech. Eng. 6 (1), 61–66.
Ly, H.B., Pham, B.T., Le, L.M., Le, T.T., Le, V.M., Asteris, P.G., 2021. Estimation of axial load-carrying capacity of concrete-filled steel tubes using surrogate models. Neural Comput. Appl. 33, 3437–3458.
Mamudur, K., Kattamuri, M.R., 2020. Application of boosting-based ensemble learning method for the prediction of compression index. J. Inst. Eng. Ser. A 101, 409–419.
Mirabbasi, R., Kisi, O., Sanikhani, H., Meshram, S.G., 2019. Monthly long-term rainfall estimation in Central India using M5Tree, MARS, LSSVR, ANN and GEP models. Neural Comput. Appl. 31, 6843–6862.
Mittal, N., Singh, U., Sohi, B.S., 2016. Modified grey wolf optimizer for global engineering optimization. Appl. Comput. Intell. Soft Comput. 7950348, 2016.
Moayedi, H., Moatamediyan, A., Nguyen, H., Bui, X.N., Bui, D.T., Rashid, A.S.A., 2020. Prediction of ultimate bearing capacity through various novel evolutionary and neural network models. Eng. Comput. 36, 671–687.
Mohammadzadeh S, D., Bazaz, J.B., Alavi, A.H., 2014. An evolutionary computational approach for formulation of compression index of fine-grained soils. Eng. Appl. Artif. Intell. 33, 58–68.
Mohammadzadeh S, D., Bazaz, J.B., Vafaee Jani Yazd, S.H., Alavi, A.H., 2016. Deriving an intelligent model for soil compression index utilizing multi-gene genetic programming. Environ. Earth Sci. 75, 262.
Mohammadzadeh S, D., Kazemi, S.F., Mosavi, A., Nasseralshariati, E., Tah, J.H.M., 2019. Prediction of compression index of fine-grained soils using a gene expression programming model. Infrastructure 4 (2), 26.
Mohammed, A., Burhan, L., Ghafor, K., Sarwar, W., Mahmood, W., 2021. Artificial neural network (ANN), M5P-tree, and regression analyses to predict the early age compression strength of concrete modified with DBC-21 and VK-98 polymers. Neural Comput. Appl. 33, 7851–7873.
Nhu, V.H., Samui, P., Kumar, D., Singh, A., Hoang, N.D., Tien Bui, D., 2020. Advanced soft computing techniques for predicting soil compression coefficient in engineering project: a comparative study. Eng. Comput. 36, s1405–s1416.
Nishida, Y., 1956. A brief note on compression index of soil. J. Soil Mech. Found Div. 82 (3). https://doi.org/10.1061/JSFEAQ.0000015.
Park, H.I., Lee, S.R., 2011. Evaluation of the compression index of soils using an artificial neural network. Comput. Geotech. 38, 472–481.
Rad, H.N., Bakhshayeshi, I., Wan Jusoh, W.A., Tahir, M.M., Foong, L.K., 2020. Prediction of flyrock in mine blasting: a new computational intelligence approach. Nat. Resour. Res. 29, 609–623.
Raghuram, G., Verma, A., 2019. Dedicated freight corridor : current challenges. In: Proceedings of the 15th World Conference on Transport Research (WCTR 2019), Mumbai, India.
Raja, M.N.A., Shukla, S.K., 2020. An extreme learning machine model for geosynthetic-reinforced sandy soil foundations. Proc. Inst. Civ. Eng. Geotech. Eng. https://doi.org/10.1680/jgeen.19.00297.
Raja, M.N.A., Shukla, S.K., 2021a. Predicting the settlement of geosynthetic-reinforced soil foundations using evolutionary artificial intelligence technique. Geotext. Geomembranes 49, 1280–1293.
Raja, M.N.A., Shukla, S.K., 2021b. Multivariate adaptive regression splines model for reinforced soil foundations. Geosynth. Int. 28 (4), 368–390.
Raja, M.N.A., Shukla, S.K., Khan, M.U.A., 2021. An intelligent approach for predicting the strength of geosynthetic-reinforced subgrade soil. Int. J. Pavement Eng. https://doi.org/10.1080/10298436.2021.1904237.
Ridha, H.M., Heidari, A.A., Wang, M., Chen, H., 2020. Boosted mutation-based Harris hawks optimizer for parameters identification of single-diode solar cell models. Energy Convers. Manag. 209, 112660.
Roy, B., Singh, M.P., 2020. An empirical-based rainfall-runoff modelling using optimization technique. Int. J. River Basin Manag. 18, 49–67.
Roy, B., Singh, M.P., Singh, A., 2021. A novel approach for rainfall-runoff modelling using a biogeography-based optimization technique. Int. J. River Basin Manag. 19, 67–80.
Samui, P., Das, S., Kim, D., Yoon, G.L., 2011. Determination of compression index for marine clay: a least square support vector machine approach. Int. J. Adv. Soft Comput. Appl. 3 (1). http://www.home.ijasca.com/vol3-1-3/.
Samui, P., Kim, D., 2017. Minimax probability machine regression and extreme learning machine applied to compression index of marine clay. Indian J. Geo-Mar. Sci. 46, 2350–2356.
Samui, P., Kim, D., Das, S., Yoon, G.L., 2012. Determination of compression index for marine clay: a relevance vector machine approach. Mar. Georesour. Geotechnol. 30, 263–273.
Sharifi, S., Abrishami, S., Gandomi, A.H., 2020. Consolidation assessment using multi expression programming. Appl. Soft Comput. 86, 105842.
Shi, X.C., Guo, Y.F., 2013. Application of genetic arithmetic and support vector machine in prediction of compression index of clay. Appl. Mech. Mater. 438–439, 1167–1170.
Sihwail, R., Omar, K., Ariffin, K.A.Z., Tubishat, M., 2020. Improved Harris hawks optimization using elite opposition-based learning and novel search mechanism for feature selection. IEEE Access 8, 121127–121145.
Simon, D., 2008. Biogeography-based optimization. IEEE Trans. Evol. Comput. 12, 702–713.
Skempton, A.W., Jones, O.T., 1944. Notes on the compressibility of clays. Q. J. Geol. Soc. 100, 119–135.
Sower, G.F., Sower, G.B., 1970. Introductory Soil Mechanics and Foundation, third ed. Macmillan, New York, USA.
Taylor, K.E., 2001. Summarizing multiple aspects of model performance in a single diagram. J. Geophys. Res. Atmos. 106, 7183–7192.
Terzaghi, K., Peck, R.B., Mesri, G., 1967. Soil Mechanics in Engineering Practice. John Wiley & Sons. Inc., New York, USA.
Tian, D., Shi, Z., 2018. MPSO: modified particle swarm optimization and its applications. Swarm Evol. Comput. 41, 49–68.
Wang, L., Wu, C., Gu, X., Liu, H., Mei, G., Zhang, W., 2020a. Probabilistic stability analysis of earth dam slope under transient seepage using multivariate adaptive regression splines. Bull. Eng. Geol. Environ. 79, 2763–2775.
Wang, L., Wu, C., Tang, L., Zhang, W., Lacasse, S., Liu, H., Gao, L., 2020b. Efficient reliability analysis of earth dam slope stability using extreme gradient boosting method. Acta Geotech 15, 3135–3150.
Wang, Z.Z., Goh, S.H., 2021. Novel approach to efficient slope reliability analysis in spatially variable soils. Eng. Geol. 281, 105989.
Wolpert, D.H., Macready, W.G., 1995. No Free Lunch Theorems for Search. Technical Report SFI-TR-95-02-010. Santa Fe Institute, Santa Fe, USA.
Wróbel, J., Kulawik, A., 2019. Calculations of the heat source parameters on the basis of temperature fields with the use of ANN. Neural Comput. Appl. 31, 7583–7593.
Zhang, W., Goh, A.T.C., 2016. Multivariate adaptive regression splines and neural network models for prediction of pile drivability. Geosci. Front. 7, 45–52.
Zhang, W., Li, Y., Wu, C., Li, H., Goh, A.T.C., Liu, H., 2020a. Prediction of lining response for twin tunnels constructed in anisotropic clay using machine learning techniques. Undergr. Space. https://doi.org/10.1016/j.undsp.2020.02.007.
Zhang, W., Wu, C., Li, Y., Wang, L., Samui, P., 2021b. Assessment of pile drivability using random forest regression and multivariate adaptive regression splines. Georisk 15, 27–40.
Zhang, W., Wu, C., Zhong, H., Li, Y., Wang, L., 2021a. Prediction of undrained shear strength using extreme gradient boosting and random forest based on Bayesian optimization. Geosci. Front. 12, 469–477.
Zhang, W., Zhang, R., Wang, W., Zhang, F., Goh, A.T.C., 2019. A multivariate adaptive regression splines model for determining horizontal wall deflection envelope for braced excavations in clays. Tunn. Undergr. Space Technol. 84, 461–471.
Zhang, W., Zhang, R., Wu, C., Goh, A.T.C., Wang, L., 2020b. Assessment of basal heave stability for braced excavations in anisotropic clay using extreme gradient boosting and random forest regression. Undergr. Space. https://doi.org/10.1016/j.undsp.2020.03.001.
Zhang, W., Zhang, Y., Goh, A.T.C., 2017. Multivariate adaptive regression splines for inverse analysis of soil and wall properties in braced excavation. Tunn. Undergr. Space Technol. 64, 24–33.
Zheng, Q., Li, R., Li, X., Shah, N., Zhang, J., Tian, F., Chao, K.M., Li, J., 2016. Virtual machine consolidated placement based on multi-objective biogeography-based optimization. Future Generat. Comput. Syst. 54, 95–122.
Zhou, Y.P., Tang, L.J., Jiao, J., Song, D.D., Jiang, J.H., Yu, R.Q., 2009. Modified particle swarm optimization algorithm for adaptively configuring globally optimal classification and regression trees. J. Chem. Inf. Model. 49, 1144–1153.